A Global Pattern of Thermal Adaptation in Marine Phytoplankton

Mridul K. Thomas *et al.*

Science **338**, 1085 (2012);
DOI: 10.1126/science.1224836

Science (print ISSN 0036-8075; online ISSN 1095-9203) is published weekly, except the last week in December, by the American Association for the Advancement of Science, 1200 New York Avenue NW, Washington, DC 20005.

A Global Pattern of Thermal Adaptation in Marine Phytoplankton

Mridul K. Thomas,[1,2]*† Colin T. Kremer,[1,3]† Christopher A. Klausmeier,[1,3] Elena Litchman[1,2]

Rising ocean temperatures will alter the productivity and composition of marine phytoplankton communities, thereby affecting global biogeochemical cycles. Predicting the effects of future ocean warming on biogeochemical cycles depends critically on understanding how existing global temperature variation affects phytoplankton. Here we show that variation in phytoplankton temperature optima over 150 degrees of latitude is well explained by a gradient in mean ocean temperature. An eco-evolutionary model predicts a similar relationship, suggesting that this pattern is the result of evolutionary adaptation. Using mechanistic species distribution models, we find that rising temperatures this century will cause poleward shifts in species' thermal niches and a sharp decline in tropical phytoplankton diversity in the absence of an evolutionary response.

Marine phytoplankton are responsible for nearly half of global primary productivity (*1*). They play essential roles in food webs and global cycles of carbon, nitrogen, phosphorus, and other elements (*2*, *3*). Empirical studies have shown that recent ocean warming has driven changes in productivity (*4*), population size (*5*), phenology (*6*), and community composition (*7*). Global ocean circulation models predict further temperature-driven reductions in phytoplankton productivity this century, with consequent decreases in marine carbon sequestration (*8*, *9*). The main mechanism that these studies have identified is indirect: Rising temperatures drive an increase in ocean stratification, which in turn leads to a decrease in nutrient supply to surface waters. However, most models do not consider the direct effects of rising temperatures on individual phytoplankton species, which experience sharp declines in growth rate above their optimum temperatures for growth. They may, therefore, underestimate the effects of warming on ecosystems.

To understand how ocean warming will directly affect marine and estuarine phytoplankton, we examined growth responses to temperature in 194 strains belonging to more than 130 species from the major phytoplankton groups (*10*). Temperature-related traits, such as the optimum temperature for growth and the thermal niche width (the temperature range over which growth rate is positive), are among the most important in ectothermic species, especially given predictions of global warming (*11*). We estimated these traits from >5000 growth rate measurements, synthesized from 81 papers published between 1935 and 2011. The strains were isolated from 76°N to 75°S, giving us exceptionally broad coverage of the latitudinal and temperature gradients (fig. S1).

Growth responses to changes in temperature are characterized by thermal tolerance curves (reaction norms). Two features of these curves are common to all ectotherms: unimodality and negative skewness (i.e., a sharper decline in fitness above the optimum temperature than below) (fig. S2) (*11*, *12*). The latter condition makes ectotherms living at their optimum temperature more sensitive to warming than cooling, with important consequences for their performance in the environment (*13*). Furthermore, there is an exponential increase in the maximum growth rate attainable with increasing temperature (across species). These curves may be described using three principal traits: maximum growth rate, optimum temperature for growth, and thermal niche width. We estimated these traits for each strain by fitting a thermal tolerance function to the data (*14*) and examined their relationships with environmental and taxonomic covariates (*10*).

Our analysis revealed large-scale patterns in thermal traits. First, strains exhibited a clear latitudinal trend in the optimum temperature for growth [Fig. 1, coefficient of determination (R^2) = 0.55, $P < 0.0001$], demonstrating the existence of a global pattern in a key microbial trait. Second, optimum temperature was even more strongly related to mean annual temperature at the isolation location (Fig. 2A, $R^2 = 0.69$, $P < 0.0001$), suggesting that temperature is a major selective agent and that adaptation to local environmental conditions occurs in marine microbes despite the potential for long-distance dispersal through ocean currents. In contrast, the width of the thermal niche was unrelated to temperature regimes. Third, strains from polar and temperate waters had optimum temperatures that were considerably higher than their mean annual temperatures, whereas tropical strains had optima closer to or lower than the mean temperatures (Fig. 2A). Finally, variation in optimum temperature and niche width was not explained by taxonomic differences above the level of genus, indicating that thermal adaptation is not highly phylogenetically constrained in this group (tables S1 and S2).

This strong trait-environment relationship suggests that microbes are adapted to the temperatures that they experience locally. However, this pattern could also occur through a correlated response to selection on other traits. To test whether the observed pattern arose as an adaptive response to variable thermal regimes, we used an eco-evolutionary model (*15*, *16*) to predict the optimum temperatures that maximize fitness at each isolation location. The model allows us to study the effects of thermal adaptation alone by forcing all other aspects of strains to be identical. Purely theoretical applications of such eco-evolutionary models have been extensive, but they have rarely been compared to quantitative field data (*17*).

In the model, strains differ only in their thermal tolerance curves (characterized by their optimum temperature) while competing for a single

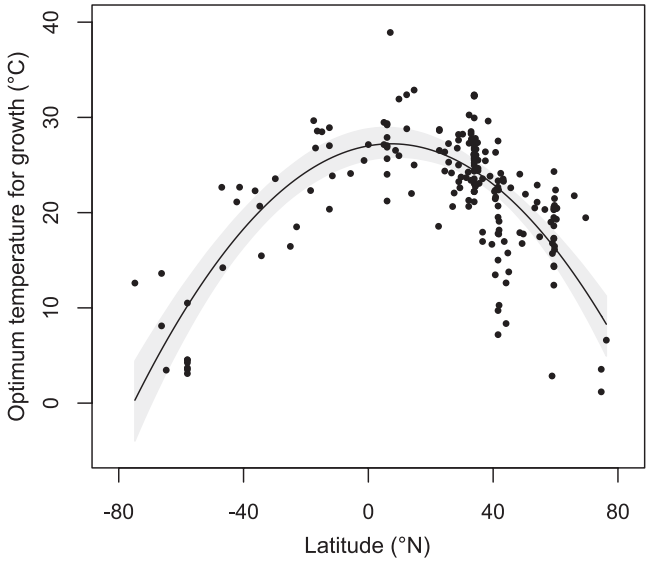

Fig. 1. Latitudinal gradient in the optimum temperature for growth of marine and estuarine phytoplankton strains (n = 194 strains, R^2 = 0.55, $P < 0.0001$). Each point represents the optimum temperature for growth of a single strain, estimated by fitting a thermal tolerance function (*14*) to the data. The regression line (black) is shown, along with 95% confidence bands (gray). Confidence bands account for asymmetric uncertainty in trait estimates using a bootstrapping algorithm [(*10*), see also fig. S9].

[1]W. K. Kellogg Biological Station, Michigan State University, Hickory Corners, MI 49060, USA. [2]Department of Zoology, Michigan State University, East Lansing, MI 48824, USA. [3]Department of Plant Biology, Michigan State University, East Lansing, MI 48824, USA.

*To whom correspondence should be addressed. E-mail: thomasmr@msu.edu

†These authors contributed equally to this work.

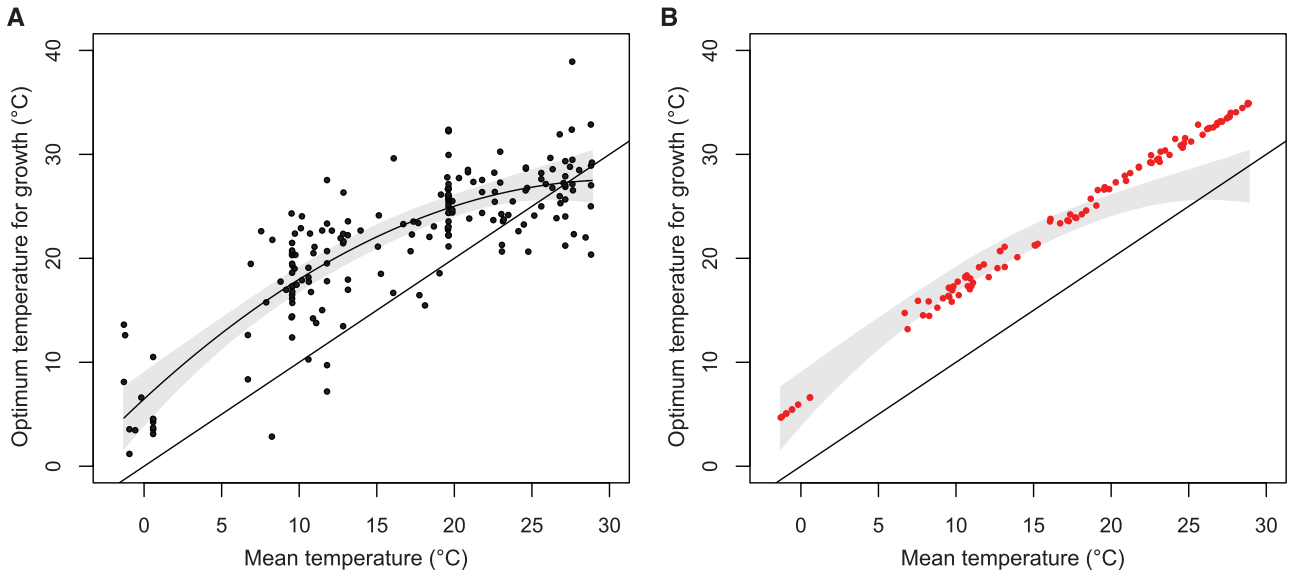

Fig. 2. Optimum temperatures for growth across a gradient of ocean temperature. (**A**) The optimum temperature of phytoplankton strains is well explained by variation in the mean annual temperature at their isolation locations ($n = 194$, $R^2 = 0.69$, $P < 0.0001$), indicating adaptation to local environmental conditions. The 1:1 line (black, straight), regression line (black, curved) and 95% confidence bands (gray) from bootstrapping are shown (*10*). The regression line shown is for the best model (table S4), which posits a quadratic relationship between mean temperature and optimum temperatures. (**B**) The eco-evolutionary model predicts evolutionarily stable optimum temperatures (red points) for each isolation location that are several degrees higher than the mean environmental temperatures (i.e., above the black line) and agree well with the data, except in the warmest waters. The confidence band from (A) is shown in gray for comparison.

nutrient. The growth rates of all strains are bounded by an exponential function that increases with temperature, an empirical relationship known as the Eppley curve (*12*). We require that each individual strain's thermal tolerance curve touch the Eppley curve at a single point, forcing maximum growth rate to become a function of optimum temperature. Niche widths are held constant across strains, because we found no significant relationship in our data set between niche width and environmental or taxonomic covariates (tables S1 and S2). Given these constraints, we allow optimum temperatures of a set of strains to evolve in response to deterministic temperature regimes. These regimes were based on model fits to a 30-year sea surface temperature time series at every isolation location (*10*, *18*). For each environment, we used an evolutionary algorithm based on quantitative genetics to identify evolutionarily stable states (ESSs) (*10*, *16*). At an ESS, the strains that persist (defined by their traits) cannot be invaded by any other strain. These temperature optima serve as a theoretical prediction of the best strategy (or strategies) at each isolation location, which we can then compare to our data as a test of thermal adaptation.

Our eco-evolutionary model predicts that optimum temperatures should increase with mean temperature and exceed it by several degrees (Fig. 2B and fig. S3). This is in agreement with the observed pattern (Fig. 2A) and bolsters the case that this relationship arises from adaptation to mean temperature. However, in regions with the highest mean temperatures (the tropics), the model predicts optima that are significantly higher than those observed. Although this discrepancy suggests that tropical strains may be less well-adapted to their environmental temperatures, we estimated that these strains are capable of persistence under the temperature regimes they experience (Figs. 2B and 3) (*19*). The difference may be a result of interactions between temperature and other factors, constraints on thermal adaptation at high temperatures, or adaptation to laboratory temperatures before measurement. Examining model predictions across a range of assumed niche widths reveals that wider niches lead to larger differences between predicted optima and the mean annual temperatures and to a decrease in the number of coexisting strains (fig. S3). These results illustrate that temperature variation can support species coexistence, although it cannot fully explain the levels of trait diversity observed in the data.

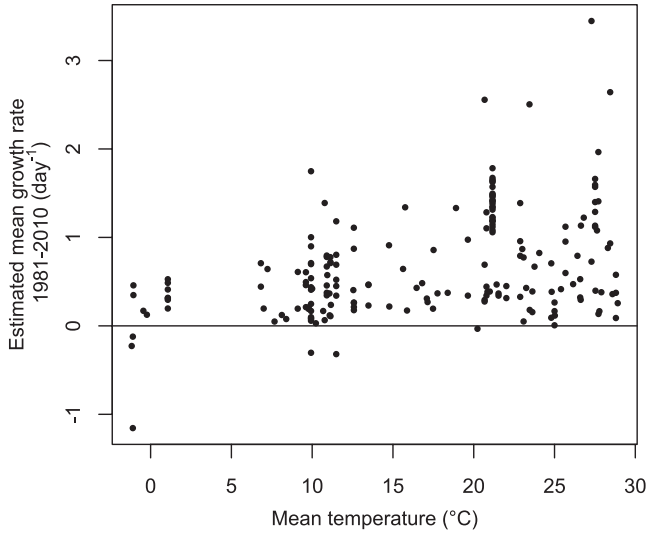

Fig. 3. Estimated mean daily growth rates of all strains at their isolation locations, between 1980 and 2010. These estimates were based on monthly temperature records (*19*) and each strain's thermal tolerance curve, and depend on the assumption that growth is limited solely by temperature. Even warm-water strains have mean growth rates exceeding zero (the horizontal line), indicating that they are capable of persisting in their environment, although their optima are below what our model predicts to be most adaptive.

Phytoplankton strains may be adapted to their current conditions, but could be negatively affected by warming oceans. Moving from the eco-evolutionary model to purely physiological mechanistic species distribution models (SDMs), we then examined whether changing environmental temperatures could alter species ranges and global diversity patterns. These models use physiological trait measurements to predict species abundances across environmental gradients (*20*) but do not account for species interactions or

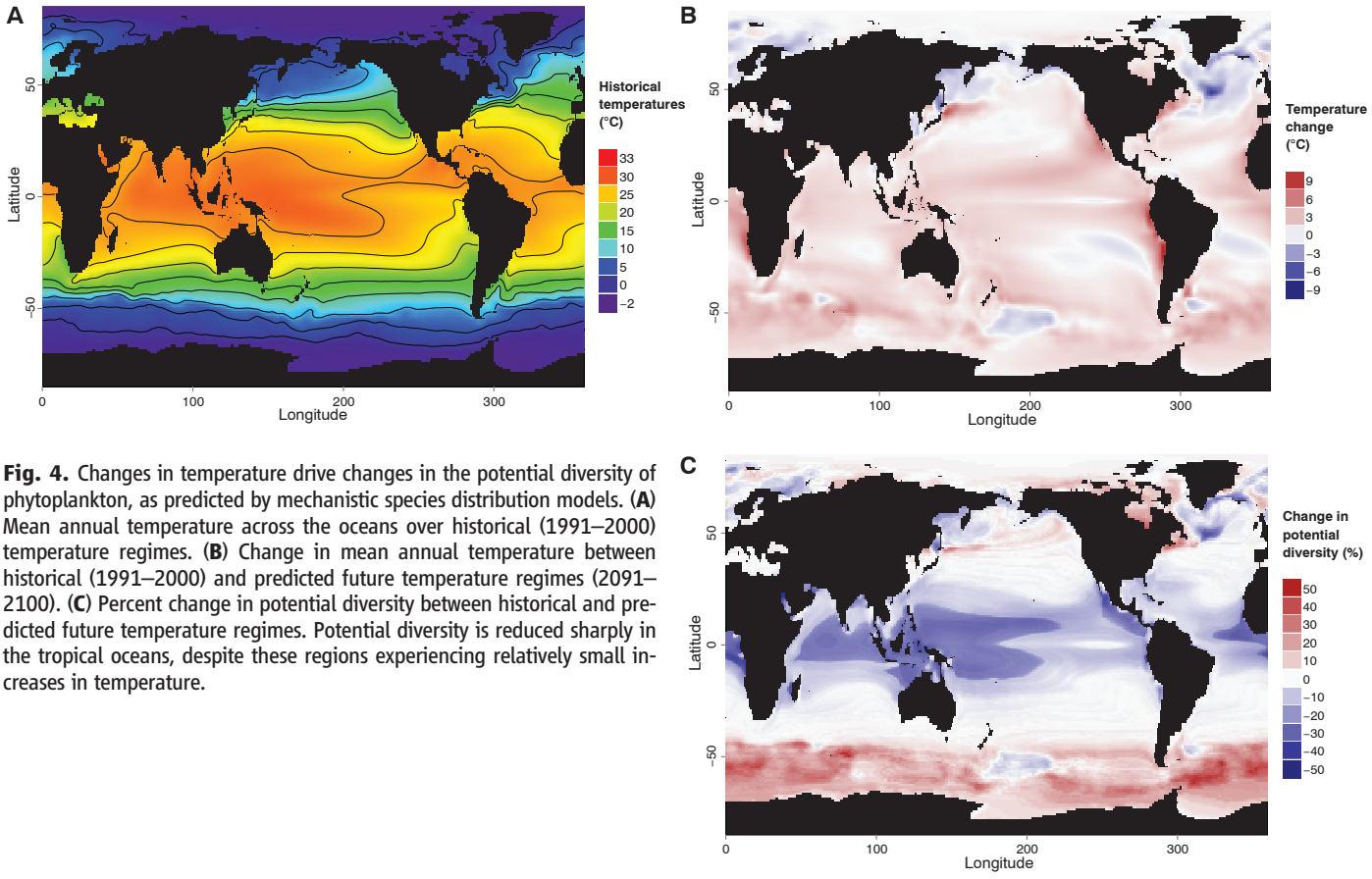

Fig. 4. Changes in temperature drive changes in the potential diversity of phytoplankton, as predicted by mechanistic species distribution models. (**A**) Mean annual temperature across the oceans over historical (1991–2000) temperature regimes. (**B**) Change in mean annual temperature between historical (1991–2000) and predicted future temperature regimes (2091–2100). (**C**) Percent change in potential diversity between historical and predicted future temperature regimes. Potential diversity is reduced sharply in the tropical oceans, despite these regions experiencing relatively small increases in temperature.

evolution. We generated growth rate predictions across the ocean for each strain represented in our data set, based on their thermal tolerance curves and a 10-year temperature time series (*10*). If the 10-year mean growth rate of a strain was positive at a location, the location was deemed to fall within its range. We repeated this using both historical (1991–2000) and future (2091–2100) temperature regimes, the latter having been predicted by a global climate model (*10*, *19*, *21*–*23*). These estimates indicate that ocean warming is likely to drive poleward shifts in strains' equatorial boundaries, although polar range boundaries remain approximately constant (fig. S4). Consequently, many strains are predicted to experience a reduction in range size (figs. S5, S6, and S12), potentially increasing extinction probabilities. Our SDMs assume that growth rates are limited solely by temperature, but other factors, such as nutrient availability, could also be incorporated if relevant trait data were available.

When the range shifts of all strains are considered in the aggregate, they can be used to predict global patterns of phytoplankton diversity change as a result of ocean warming (Fig. 4) (*24*). In order to do this, we calculated "potential diversity," defined as the number of phytoplankton strains (out of the 194 in our data set) theoretically capable of growing at a location, assuming that temperature is the sole limiting factor (figs. S7 and S8). A comparison of potential diversity patterns under both historical and future temperature regimes shows that temperature change may drive a large reduction in tropical phytoplankton diversity over the course of this century. Approximately one-third of contemporary tropical strains are unlikely to persist there in 2100 (Fig. 4C), despite a change in mean temperature of only ~2°C (Fig. 4, A and B). High latitudes may experience small increases in potential diversity, as a result of poleward shifts in strain ranges. Rising temperatures have the strongest effect on tropical strains, because tropical optima are close to current mean temperatures (Fig. 2A) and thermal tolerance curves are negatively skewed. Small increases in temperature can therefore lead to sharp declines in growth rate. A decrease in diversity is likely to have a strong impact on tropical ecosystems, because biodiversity loss is a major cause of ecosystem change (*25*). One possible consequence is a decrease in tropical primary productivity, which could occur through two distinct mechanisms: the loss of highly productive species or a decrease in complementarity (*26*, *27*).

Our findings lend support to the hypothesis that tropical communities are most vulnerable to increases in temperature (*28*). However, the existence of high genetic diversity within species, as has been noted in some cases (*29*), may prevent the loss of entire species. Adaptation to changing temperatures may mitigate some of the predicted losses in diversity, particularly in rapidly reproducing taxa such as phytoplankton. The evolution of thermal tolerance has been examined in a few taxa, including phytoplankton (*30*–*32*), but we currently lack the information necessary to accurately model the consequences of evolutionary change on ecosystem processes (*33*, *34*). In the case of phytoplankton, we need estimates of rates of adaptation to high temperature stress in a variety of taxa, as well as an examination of the evolutionary constraints and trade-offs that may be associated with this. Characterizing these constraints will allow us to make improved forecasts of species survival and may prove critical for understanding the fate of tropical communities and oceanic ecosystems.

References and Notes

1. C. B. Field, M. J. Behrenfeld, J. T. Randerson, P. G. Falkowski, *Science* **281**, 237 (1998).
2. A. C. Redfield, *Am. Sci.* **46**, 205 (1958).
3. P. G. Falkowski, R. T. Barber, V. Smetacek, *Science* **281**, 200 (1998).
4. M. J. Behrenfeld *et al.*, *Nature* **444**, 752 (2006).
5. D. G. Boyce, M. R. Lewis, B. Worm, *Nature* **466**, 591 (2010).
6. M. Edwards, A. J. Richardson, *Nature* **430**, 881 (2004).
7. X. A. G. Morán, Á. López-Urrutia, A. Calvo-Díaz, W. K. W. Li, *Glob. Change Biol.* **16**, 1137 (2010).
8. L. Bopp *et al.*, *Global Biogeochem. Cycles* **15**, 81 (2001).
9. M. Steinacher *et al.*, *Biogeosciences* **7**, 979 (2010).
10. Materials and methods are available as supplementary materials on *Science* Online.

11. J. G. Kingsolver, *Am. Nat.* **174**, 755 (2009).
12. R. W. Eppley, *Fish Bull.* **70**, 1063 (1972).
13. T. L. Martin, R. B. Huey, *Am. Nat.* **171**, E102 (2008).
14. J. Norberg, *Limnol. Oceanogr.* **49**, 1269 (2004).
15. S. A. H. Geritz, É. Kisdi, G. Meszéna, J. A. J. Metz, *Evol. Ecol.* **12**, 35 (1997).
16. P. A. Abrams, *Ecol. Lett.* **4**, 166 (2001).
17. J. C. Stegen, R. Ferriere, B. J. Enquist, *Proc. Biol. Sci.* **279**, 1051 (2011).
18. R. W. Reynolds *et al.*, *J. Clim.* **20**, 5473 (2007).
19. R. W. Reynolds, N. A. Rayner, T. M. Smith, D. C. Stokes, W. Wang, *J. Clim.* **15**, 1609 (2002).
20. M. R. Kearney, W. Porter, *Ecol. Lett.* **12**, 334 (2009).
21. Intergovernmental Panel on Climate Change (IPCC), *Climate Change 2007: The Physical Science Basis. Contribution of Working Group I to the Fourth Assessment Report of the Intergovernmental Panel on Climate Change*, S. Solomon *et al.*, Eds. (Cambridge Univ. Press, Cambridge, 2007).
22. N. Nakićenović *et al.*, *Special Report on Emissions Scenarios: A Special Report of Working Group III of the Intergovernmental Panel on Climate Change*, N. Nakićenović, R. Swart, Eds. (Cambridge Univ. Press, Cambridge, 2000); www.osti.gov/energycitations/product.biblio.jsp?osti_id=15009867.
23. T. Delworth *et al.*, *J. Clim.* **19**, 643 (2006).
24. D. W. McKenney, J. H. Pedlar, K. Lawrence, K. Campbell, M. F. Hutchinson, *Bioscience* **57**, 939 (2007).
25. D. U. Hooper *et al.*, *Nature* **486**, 105 (2012).
26. D. Tilman, D. Wedin, J. Knops, *Nature* **379**, 718 (1996).
27. P. B. Reich *et al.*, *Science* **336**, 589 (2012).
28. C. A. Deutsch *et al.*, *Proc. Natl. Acad. Sci. U.S.A.* **105**, 6668 (2008).
29. K. Härnström, M. Ellegaard, T. J. Andersen, A. Godhe, *Proc. Natl. Acad. Sci. U.S.A.* **108**, 4252 (2011).
30. A. F. Bennett, R. E. Lenski, in *In the Light of Evolution. Volume 1. Adaptation and Complex Design*, J. C. Avise, F. J. Ayala, Eds. (National Academies Press, Washington, DC, 2007), pp. 225–238.
31. J. L. Knies, R. Izem, K. L. Supler, J. G. Kingsolver, C. L. Burch, *PLoS Biol.* **4**, e201 (2006).
32. I. E. Huertas, M. Rouco, V. López-Rodas, E. Costas, *Proc. Biol. Sci.* **278**, 3534 (2011).
33. S. L. Chown *et al.*, *Clim. Res.* **43**, 3 (2010).
34. M. J. Angilletta Jr., R. S. Wilson, C. A. Navas, R. S. James, *Trends Ecol. Evol.* **18**, 234 (2003).

Acknowledgments: This research was supported by NSF (grants DEB-0845932, DEB-0845825, and OCE-0928819), including the BEACON Center for the Study of Evolution in Action (grant DBI-0939454) and a Graduate Research Fellowship to C.T.K., as well as a grant from the James S. McDonnell Foundation. K. Edwards and N. Swenson provided statistical advice, and J. Lennon, G. Mittelbach, and E . Miller provided comments on the manuscript. The trait data presented are shown in table S5, and the collated growth rate data are in table S6. Also thanks to NOAA/OAR/ESRL PSD, Boulder, CO, USA, for NOAA_OI_SST_V2 data provided at their Web site, www.esrl.noaa.gov/psd/. This is W. K. Kellogg Biological Station contribution number 1694. E.L. and M.K.T. conceived the original idea; M.K.T. collected the growth-temperature data; M.K.T. and C.T.K. analyzed the data; C.T.K. and C.A.K. developed and C.T.K. analyzed the eco-evolutionary model; M.K.T. and C.T.K. ran the mechanistic species distribution models; and M.K.T., C.T.K., and E.L. wrote and C.A.K. commented on the manuscript.

Supplementary Materials

www.sciencemag.org/cgi/content/full/science.1224836/DC1
Materials and Methods
Figs. S1 to S12
Tables S1 to S6
References (*35*–*135*)

17 May 2012; accepted 10 October 2012
Published online 25 October 2012;
10.1126/science.1224836

Decoding Human Cytomegalovirus

Noam Stern-Ginossar,[1] Ben Weisburd,[1] Annette Michalski,[2]* Vu Thuy Khanh Le,[3] Marco Y. Hein,[2] Sheng-Xiong Huang,[4] Ming Ma,[4] Ben Shen,[4,5,6] Shu-Bing Qian,[7] Hartmut Hengel,[3] Matthias Mann,[2] Nicholas T. Ingolia,[1]† Jonathan S. Weissman[1]*

The human cytomegalovirus (HCMV) genome was sequenced 20 years ago. However, like those of other complex viruses, our understanding of its protein coding potential is far from complete. We used ribosome profiling and transcript analysis to experimentally define the HCMV translation products and follow their temporal expression. We identified hundreds of previously unidentified open reading frames and confirmed a fraction by means of mass spectrometry. We found that regulated use of alternative transcript start sites plays a broad role in enabling tight temporal control of HCMV protein expression and allowing multiple distinct polypeptides to be generated from a single genomic locus. Our results reveal an unanticipated complexity to the HCMV coding capacity and illustrate the role of regulated changes in transcript start sites in generating this complexity.

The herpesvirus human cytomegalovirus (HCMV) infects the majority of humanity, leading to severe disease in newborns and immunocompromised adults (*1*). The HCMV genome is ~240 kb with estimates of between 165 and 252 open reading frames (ORFs) (*2*, *3*). These annotations likely do not capture the complexity of the HCMV proteome (*4*) because HCMV has a complex transcriptome (*5*, *6*), and genomic regions studied in detail reveal noncanonical translational events, including regulatory (*7*) and overlapping ORFs (*8*–*11*). Defining the full set of translation products—both stable and unstable, the latter with potential regulatory/antigenic function (*12*)—is critical for understanding HCMV.

To identify the range of HCMV-translated ORFs and monitor their temporal expression, we infected human foreskin fibroblasts (HFFs) with the clinical HCMV strain Merlin and harvested cells at 5, 24, and 72 hours after infection using four approaches to generate libraries of ribosome-protected mRNA fragments (Fig. 1A and table S1). The first two measured the overall in vivo distribution of ribosomes on a given message; infected cells were either pretreated with the translation elongation inhibitor cycloheximide or, to exclude drug artifacts, lysed without drug pretreatment (no-drug). Additionally, cells were pretreated with harringtonine or lactimidomycin (LTM), two drugs with distinct mechanisms, which lead to strong accumulation of ribosomes at translation initiation sites and depletion of ribosomes over the body of the message (Fig. 1A) (*13*–*15*). A modified RNA sequencing protocol allowed quantification of RNA levels as well as identification of 5′ transcript ends by generating a strong overrepresentation of fragments that start at the 5′ end of messages (fig. S1) (*16*).

The ability of these approaches to provide a comprehensive view of gene organization is illustrated for the UL25 ORF: A single transcript start site is found upstream of the ORF (Fig. 1A, mRNA panel). Harringtonine and LTM mark a single translation initiation site at the first AUG downstream of the transcript start (Fig. 1A, Harr and LTM). Ribosome density accumulates over the ORF body ending at the first in-frame stop codon (Fig. 1A, CHX and no-drug). In the no-drug sample, excess ribosome density accumulates at the stop codon (Fig. 1A, no-drug) (*14*).

Examination of the full range of HCMV translation products, as reflected by the ribosome footprints, revealed many putative previously unidentified ORFs: internal ORFs lying within existing ORFs either in-frame, resulting in N-terminally truncated translation products (Fig. 1B), or out of frame, resulting in entirely previously unknown polypeptides (Fig. 1C); short uORFs (upstream ORFs) lying upstream of canonical ORFs (Fig. 2A); ORFs within transcripts antisense to canonical ORFs (Fig. 2B); and previously unidentified short ORFs encoded by distinct transcripts (Fig. 2C). For all of these categories, we also observed ORFs starting at near-cognate codons (codons differing from AUG by one nucleotide), especially CUG (Fig. 2D).

HCMV expresses several long RNAs lacking canonical ORFs, including β2.7, an abundant RNA, which inhibits apoptosis (*17*). In agreement with β2.7's observed polysome association (*18*), multiple short ORFs are translated from this RNA (Fig. 2E and fig. S2), and the corresponding proteins for two of these ORFs were detected by means of high-resolution MS (Fig. 2E). Although the translation efficiency

[1]Department of Cellular and Molecular Pharmacology, Howard Hughes Medical Institute, University of California, San Francisco, San Francisico, CA 94158, USA. [2]Department of Proteomics and Signal Transduction, Max Planck Institute of Biochemistry, Martinsried D-82152, Germany. [3]Institut für Virologie, Heinrich-Heine-Universität Düsseldorf, 40225 Düsseldorf, Germany. [4]Department of Chemistry, Scripps Research Institute, 130 Scripps Way #3A2, Jupiter, FL 33458, USA. [5]Department of Molecular Therapeutics, Scripps Research Institute, 130 Scripps Way #3A2, Jupiter, FL 33458, USA. [6]Natural Products Library Initiative at The Scripps Research Institute, Scripps Research Institute, 130 Scripps Way #3A2, Jupiter, FL 33458, USA. [7]Division of Nutritional Sciences, Cornell University, Ithaca, NY 14853, USA.

*To whom correspondence should be addressed. E-mail: michalsk@biochem.mpg.de (A.M.); weissman@cmp.ucsf.edu (J.S.W.)

†Present address: Department of Embryology, Carnegie Institute for Science, Baltimore, MD 21218, USA.

www.sciencemag.org/cgi/content/full/science.1224836/DC1

Supplementary Materials for

A Global Pattern of Thermal Adaptation in Marine Phytoplankton

Mridul K. Thomas,* Colin T. Kremer, Christopher A. Klausmeier, Elena Litchman

*To whom correspondence should be addressed. E-mail: thomasmr@msu.edu

Published 25 October 2012 on *Science* Express
DOI: 10.1126/science.1224836

This PDF file includes:

Other Supplementary Materials for this manuscript include the following:
(available at www.sciencemag.org/cgi/content/full/science.1224836/DC1)

1 Materials and Methods

We provide additional details on methods, statistical analyses, models, and data sources in this supplement. A graphical overview of the various data sets and analyses composing this project can be seen in Figure S11. §1.1 describes the selection criteria used to identify the growth rate data used in this study. §1.2 details the statistical procedures used to fit and describe the thermal tolerance curves. §1.3 outlines the bootstrapping approach used to appropriately account for uncertainty in estimates of thermal traits. §1.4 covers the statistical analysis used to characterize temperature regimes. §1.5 describes statistical methods used to demonstrate trait-environment relationships while accounting for trait uncertainty. §1.6 explains our analysis of trait variation as a function of taxonomy. §1.7 describes the structure and analysis of our eco-evolutionary model. §1.8 provides extra details on the data and methods employed in our species distribution models. §1.9 lists the various pieces of computational software we employed.

1.1 Curve selection criteria

We assembled a data set containing growth rate measurements of marine and estuarine phytoplankton at different temperatures that have been published over the past century. All measurements were digitized using g3data *(35)*. Strains were treated as independent, due to the existence of considerable intraspecific variation and uncertainty in species boundaries for some taxa.

Several criteria were used to determine the inclusion of species/strain data in our analyses.

1) To facilitate comparisons across studies we only included data for growth rates measured in units that could be converted to specific growth rate.
2) Because we were primarily concerned with estimating the temperature at which strains/species achieve their maximum growth rates, we rejected curves where the largest measured growth rate occurred at the lowest or highest temperature considered.
3) Curves with fewer than four measured growth rates were excluded, as were curves showing strong bimodality, which we attributed to imprecise experimental measurements.
4) Where curves were measured under different experimental conditions (salinity, nutrient limitation, light levels, day length), we preferentially selected curves meeting the following conditions:
    a. Salinity between 30 and 40 parts per thousand.
    b. Light levels greater than or equal to 100 microeinsteins.$m^{-2}.s^{-1}$.
    c. Not experimentally limited by nutrients
    d. Day lengths of greater than or equal to 10 hours.

    When no curves for a particular isolate satisfied these experimental constraints, we settled for using data from the curve(s) that were closest to the desired light and salinity levels.
5) We considered only marine and estuarine strains not isolated from inland waters.

After applying these criteria, we had data for a total of 252 separate curves, divided among 194 isolates/strains belonging to approximately 130 species, from 111 unique isolation locations ranging in latitude from 76°N to 75°S (Fig. S1, Table S5).

1.2 Statistical analysis of thermal tolerance curves

Temperature dependent specific growth rates can be described by the following equation[16]:

$$f(T) = ae^{bT}\left[1 - \left(\frac{T - z}{w/2}\right)^2\right] \quad \text{(S.1)}$$

Here specific growth rate f is an explicit function of temperature, T. The shape of the thermal tolerance curve is controlled by two important species traits, z and w. The range of temperatures over which growth rate is positive, or the thermal niche width, is given by w. Species trait z determines the location of the maximum of the quadratic portion of this function. In the case where parameter $b = 0$, this value is identical to the temperature at which a species achieves its maximum growth rate. However, when b is non-zero, the maximum value of S.1 falls above (or potentially below, $b < 0$) the value of z, and can be found through numerical optimization.

Norberg *(14)* fixed parameters a and b according to the values of the Eppley curve *(12)*, an exponential relationship thought to provide the community-level upper bound (95% quantile) on phytoplankton growth as a function of temperature. However, in fitting growth curves to data for individual strains, we recognized that species may not strictly follow this community level constraint, potentially due to the effects of other constraints such as light or nutrient limitation. For this reason, we allowed a and b to be free parameters, fit simultaneously with z and w.

To describe the growth data for each isolate, we used a maximum likelihood approach, such that the mean growth rate at a given temperature followed equation (S.1),

$$\mu = f(T) + \mathcal{N}(0, \sigma^2) \quad \text{(S.2)}$$

Here observational error was described by a normal distribution with a mean of zero and variance of σ^2.

1.3 Determining physiological parameter uncertainty

While confidence intervals for the point estimates of the parameters of (S.1) were easy to obtain, it was not straightforward to determine uncertainty for implicit properties such as the temperature at which growth rate is maximized (or, the 'optimum temperature'). Yet, this was the property that we were mainly interested in, leading us to adopt a parametric bootstrapping approach.

We used a Monte Carlo approach such that for each thermal tolerance curve having n data points, we simulated n new data points, drawn from a normal distribution such that:

1) The mean of the distribution corresponds to the value of (S.1) at each of the original experimental temperatures, given the coefficients previously estimated for the original curve.
2) The standard deviation of the distribution, σ, was obtained by adjusting the original maximum likelihood estimate, $\hat{\sigma}$, to account for uncertainty in its estimation *(36)*:

$$\hat{\sigma}^2 = \sigma^2 \sqrt{(n-1)/X} \qquad \text{(S.3)}$$

where n is the number of points, and X is a random number drawn from the χ^2 distribution having (n - 1) degrees of freedom.

Equation (S.1) was then fit to the simulated data using maximum likelihood estimation, and the new parameter values, as well as the numerically estimated optimum temperature, were retained. Repeating this process a total of 10,000 times (for each isolate), yielded bootstrapped distributions of all parameter estimates. From these distributions we calculated the 95% confidence intervals as the range between the 2.5th and 97.5th quantiles. These estimates of uncertainty were vital for subsequent analyses, as they allowed us to appropriately account for the inherent differences in uncertainty between different isolates expected to arise any time that data are synthesized across many individual studies.

1.4 Environmental data analysis

To provide the environmental data necessary for investigating trait-environment relationships, we turned to historical sea surface temperature (SST) estimates available through NOAA as ¼ degree, AVHRR/AMSR+AVHRR daily optimum interpolation SST *(18)*. These data covered the period between 1981 and 2010. Because of the fine spatial resolution of these data, we were able to closely match the location of each isolate to the nearest location having SST data, minimizing error due to spatial variation. When more than one ¼ degree location was equidistant from an isolation location, a specific grid location was selected randomly from the various options. Our initial set of 111 distinct isolation locations were matched in this manner to a set of 106 distinct SST locations. We then assembled time series of sea surface temperature at each of these locations from Sept. 1st, 1981 to Jan. 18th, 2011. Temperature regimes were described by fitting the following modified sinusoidal function to the entire 30-year time series at each location, again using a maximum likelihood approach:

$$T(t) = \phi + r\left[\sin\left(\frac{\pi}{365}(t+\beta)\right)\right]^{2\alpha} \qquad \text{(S.4)}$$

In this model, $|r|$ describes the range of temperatures achieved, while ϕ provides the maximum ($r < 0$) or minimum ($r > 0$) temperature. Parameters α and β describe the skewness and temporal shift of the temperature oscillations, respectively. The addition of the α parameter extends a typical sine function to capture asymmetrical seasonality (for example, longer warm periods than cold periods). Note however, that for α = ½, equation (S.4) reduces to an ordinary sinusoidal model. These regressions generally fit the data well (n = 106 time series, mean R^2 of 0.81, standard deviation of 0.17). Note that due to

the inherent assumption of observation error, standard regression models describing temperature time series (such as S.4) will always underestimate the extreme range of temperatures.

We calculated mean temperatures and temperature ranges directly from time series data for each location, as well as the mean and range of the deterministic model fit to the time series. These results are used subsequently in establishing trait-environment relationships, and (in the case of the deterministic model) to describe realistic temperature fluctuations in our eco-evolutionary model.

1.5 Trait-environment regression randomizations

We wanted to calculate regressions relating latitude and mean temperature to phytoplankton optimum temperatures, while accounting for the varying levels of uncertainty attached to each estimate of optimum temperature. Typically meta-analyses handle this issue by performing a weighted regression, using the inverse of the uncertainty associated with each data point. This approach implicitly assumes that the uncertainty around each point estimate is symmetric, which was clearly not the case for our traits (see for example the bootstrapped confidence intervals around point estimates of optimum temperatures, Fig. S9). Consequently, we employed a different approach using resampling techniques, which, to be useful, needed to provide: 1) regression coefficients, 2) uncertainty in regression fit, and 3) a means of comparing the fits of a set of alternative models. Note that we wanted to account for two kinds of uncertainty in this process, both the uncertainty arising from error in estimates of optimum temperature and the uncertainty associated with fitting a regression to data.

Recall that during our earlier parametric bootstrapping calculations we obtained 10,000 estimates of the thermal optimum of each of $n = 194$ isolates, via a process that is independent across isolates. For the ith iteration of this resampling procedure, we did the following:

1) Drew the ith value (out of 10,000) from each of the 194 distributions of estimated thermal optima. This captured error associated with uncertainty in our thermal optima estimates.
2) Fit each of the regression models under consideration to this randomized data
3) Performed standard model comparison of these regressions, saving the Akaike weights associated with each model. Akaike weights capture the relative likelihood of a model, given the data and set of competing models under consideration *(37)*.
4) To capture uncertainty associated with each of these models, we conducted residual resampling, associating each predicted value from a given regression with a new residual, and repeating the regression.
5) Saved the estimates of the resulting regression coefficients.

This process was repeated a total of 10,000 times across all of the bootstrapped optimum temperature values. The result was a distribution of parameter estimates for each of the regression fits. From these we calculated confidence intervals on the regression

parameters, as well as confidence bands for the relationships as a whole. Finally, we determined the model(s) with the most explanatory power by looking at the average Akaike weight (across the 10,000 replicates) associated with each.

This method was used to examine the relationship between optimum temperature and latitude (having considering linear and quadratic models), resulting in Figure 1. A more extensive set of models was examined when considering the relationship between optimum temperature and the mean and range of environmental temperatures. The set of models considered, as well as the corresponding average Akaike weights, are provided in Table S4, while the model receiving the greatest weight is presented in Figure 2A.

1.6 Taxonomic model comparison

As the genetic sequence data necessary to construct a complete phylogeny for the species in our dataset were not available, we tested for a taxonomic signal *(38, 39)* in optimum temperature and temperature niche width. Strains were classified according to Algaebase *(40)* supplemented with a few entries from ITIS *(41)*. In the case of optimum temperature, we constructed a full linear mixed model containing environmental parameters (mean annual temperature) as fixed effects and all taxonomic levels (from domain to strain) as nested random effects. This was compared against a set of models that omitted each individual taxonomic level using Akaike Information Criterion (AIC), a tool used in information theoretic approaches to model selection that measures goodness of fit of a statistical model (Table S1). In the case of niche width, the models contained taxonomic levels, but not environmental covariates, as none explained variation in niche width. A summary of the full models is in Table S2. Analyses were repeated using an alternate method in which taxonomic levels were added in sequentially and compared against the previous model. The results did not change our conclusions, though we were unable to test for the effect of Domain on either trait.

1.7 Eco-evolutionary modeling

1.7.1 Model setup.

We used a version of an eco-evolutionary modeling framework called adaptive dynamics *(15, 16)* to determine the thermal strategy or strategies that represent evolutionary equilibria for each temperature regime represented in our dataset. All parameters used in the subsequent model are presented in Table S3, along with their units and the numerical values used in our simulations, where appropriate. Our approach consisted of defining the per capita growth rate of phytoplankton strain i as a function of its traits (focusing on z_i) and environment (nutrient level and temperature) as follows:

$$\frac{1}{N_i}\frac{dN_i}{dt} = \mu(z_i, T)\frac{R}{R+k} - m(T) \qquad \text{(S.5)}$$

In this model, strains exhibit a temperature dependent growth rate $\mu(z_i, T)$, equation (S.7), subject to the availability of resource R and half-saturation constant k. Given that very

little is known about the interactive effects of temperature and resource dynamics, we treated resource dynamics as simply as possible (algebraically):

$$R(t) = R_{in} - \sum_i N_i(t) \tag{S.6}$$

Growth rates were taken to be both trait and temperature dependent:

$$\mu(z_i, T(t)) = 0.81 e^{0.0631 T(t)} \left[1 - \left(\frac{T(t) - z_i}{w/2} \right)^2 \right] \tag{S.7}$$

where temperature dynamics follow (S.4). This equation is similar to that of Norberg *(14)* and (S.1), but instead of using Eppley's original coefficients *(12)* we made use of more recently refined parameters *(42)*. The value of this function (S.7) depends critically on strain traits z_i and w, which are the temperature at which a strain touches the Eppley curve and the strain's thermal niche width, respectively. Three different values of niche width w were investigated, approximately spanning the range of niche widths that we could estimate from literature data with confidence (6.1 to 33.9 °C). Trait z_i can be interpreted as the temperature at which a strain's thermal tolerance curve lies tangent to the Eppley curve. To obtain predictions of thermal optima comparable to those in the rest of the paper, we used numerical methods to determine the temperature at which (S.7) reaches its maximum. In addition to depending on trait z_i, growth rate depends on the temperature, $T(t)$, which varies over time following (S.4) with specific parameters that differ depending on the particular environment under consideration (see section 'Environmental data analysis'). In the model, all strains experience a temperature dependent mortality rate, $m(T)$ that is 5% of the Eppley curve (i.e. 5% of the maximum growth rate), regardless of their traits.

Finally, we allowed strains to evolve or change their trait value z_i dynamically through time according to *(16)*:

$$\frac{dz_i}{dt} = \varepsilon \frac{d}{dz_i} \left[\frac{1}{N_i} \frac{dN_i}{dt} \right] \tag{S.8}$$

In this model, the change in trait over time is driven by the fitness gradient of a strain, or how much the per capita growth rate (fitness) of a strain increases (or decreases) with small changes in its trait value. This rate is scaled by parameter ε, which we take to be small so that traits are approximately constant within a period, effectively forcing the separation of time scales between ecological and evolutionary dynamics *(43)*. Equation (S.8) is analogous to the breeder's equation drawn from quantitative genetics *(16)*.

1.7.2 Predictions of optimal trait values - adaptive dynamics simulations.

Together, (S.5-S.8) provide a system of differential and algebraic equations that can be analyzed numerically and used to predict the evolutionary stable strategies (ESSs), or equilibrium trait value(s), of phytoplankton species in a given environment. These

predictions allowed us to test whether our understanding of the interaction between physiological constraints and environmental variation, and ecology and evolution, is enough to predict trait-environment relationships observed in the real world. Eco-evolutionary models have rarely been used as a source of predictions for comparing with data, with notable exceptions *(17, 44, 45)*.

We performed eco-evolutionary simulations for each of the 106 distinct historical temperature regimes earlier matched to isolates. The temperature forcing (S.4) for these simulations are parameterized using the results from the earlier section 'Environmental data analysis'. For each location, we started with four species having initial trait values z_i uniformly distributed across that site's range of temperatures. We then used Wolfram Mathematica version 8 to numerically solve this system of eight differential equations forward in time, until they reached their dynamic attractor. During this process, the trait and population dynamics of each strain were monitored, such that:

1) If the trait values of any two strains converged on each other to within $1x10^{-4}$, their biomasses were summed, and they were merged into a single pair of equations, and
2) If the biomass of an individual strain integrated over one time period fell below $1x10^{-12}$, it was considered to have suffered extinction and its pair of equations was removed from the system.

Once this system reached its dynamic attractor, we took the average value of z_i over a single period for each of the remaining strains and determined the temperature at which the corresponding thermal tolerance curve achieved its maximum growth rate. This provided us with estimates of the ESS optimum temperatures and diversity of coexisting strains, matched to that particular environment (Fig. S10).

We then repeated this process across each set of environmental conditions, for three different settings of niche widths (see Fig. S3 and parameters in Table S3). For environments where the ESS consisted of a single strain, we found that its optimum temperature was consistently higher than the mean annual temperature by a factor determined by the strain's niche width. These strains all shared the property that their z (the temperature at which their thermal tolerance curves were tangent to the Eppley curve) exactly matched the mean annual temperature they experienced. In other words, their most adaptive strategy is to have values of z such they grew as fast as theoretically possible at the mean annual temperature. However, because their thermal tolerance curves are bounded by an increasing function, the value of z is not the same as the temperature at which each strain achieves its own fastest growth rate, usually defined as its optimum temperature (see Fig. S2). The difference between the temperatures at which these two points occur is determined by the niche width, explaining the offset we observe.

This particular method of eco-evolutionary modeling is only one of several methods that could be applied to this problem. We selected it because under some situations, such as with fluctuating environments, it can be more computationally tractable than more traditional 'Adaptive Dynamics' methods. Additionally, in future

work it can easily be extended to account for trait change on ecological time scales *(16, 46)* by increasing ε, enabling us to potentially study evolutionary responses to climate change within the same framework. It is worth noting that the maximum number of coexisting strains that can be identified using this approach is constrained by the total number of initial strains (four in our case), so it remains possible that temperature variation could support higher levels of diversity than we determined in this study. However, this seems unlikely as the most diverse result obtained consisted of only three strains.

1.8 Species distribution modeling.

The thermal tolerance curve of a given species allowed us to calculate its growth rate under any given environmental temperature. A time series of environmental temperatures can thus be converted into a time series of estimated growth rates. We can then calculate the average per-capita growth rate of a species over the duration of the time series, in the absence of other limiting factors. Environments in which this growth rate was positive were considered to be within the geographic limits of the species' fundamental niche, with respect to temperature. Repeating this exercise for time series data across the world oceans for each strain in our study, we estimated the spatial extent of the strain's fundamental temperature niche. We then examined how these species distributions differ given historical and predicted future thermal regimes.

1.8.1 Data sets

For this analysis we drew on two additional sources of sea surface temperature data:

1) Monthly mean historical sea surface temperatures, 1° x 1° *(19)*, and
2) Projections of future temperature regimes obtained from the NOAA GFDL CM2.1 *(23, 47)*. This model was driven with the SRES A2 emissions scenario, characterised by rapid population growth and heterogeneous development *(22)*. This dataset contained global ocean temperature projections from 2001 to 2100, with a spatial resolution of 1° x 1° and a temporal resolution of 1 month. We focused on the final ten-year period from 2091-2100, at the end of which CO_2 concentrations reach 800 ppm.

These data sets have similar resolutions, but use different spatial grids (fixed versus Gaussian, respectively). To generate predictions that are directly comparable between historical and future temperature regimes we used bounded universal kriging to conduct spatial interpolations, basing the requisite theoretical variograms on Gaussian model fits to the semivariograms of each spatial data set. Because the world is round, kriging methods applied to global data sets based on latitude/longitude are prone to boundary effects. We minimized this problem for our kriging by generating two different interpolations, where the longitudinal boundary fell at 0° and 180°, respectively. We then generated a corrected interpolation by combining these results, while excluding edge values within the local neighbourhood size employed in the bounded universal kriging. This interpolation allowed us to generate spatially congruent data sets, based on which we could make valid area, range shift and diversity comparisons.

1.8.2 Range shift estimates.

Using the above methods, we generated spatial predictions of the fundamental temperature niches (i.e. all locations where its growth rate averaged over its thermal environment was positive) or species distributions of all 194 strains in our data set, for both historical and future environments. These calculations were performed without allowing for strain evolution, such that the traits of contemporary strains were assumed to be the same traits with which they will confront future environments. Comparing these results enabled us to quantify shifts in the fundamental range of these species, including changes in both range size and range position (see Figs. S4–S6, and Fig. S12 for a complete set of range maps).

1.8.3 Diversity change estimates.

When examined in the aggregate, species distribution models allowed us to examine broad-scale patterns in potential diversity. We generated potential diversity predictions for each ocean location by calculating the number of strain ranges it fell within, under both historical and predicted future temperature regimes. Historical diversity estimates were kriged (see above) to make them comparable to estimates of future diversity. The historical diversity at each location was then subtracted from future diversity to generate predictions of diversity change over the 100-year time period (see Figs. S7 and S8).

1.9 Software employed.

All statistical analyses were performed using R *(48)*, as well as the following packages: bbmle *(49)* (for maximum likelihood regressions and model comparison), reshape *(50)* (for data manipulation), ggplot2 *(51)* (for figure creation), ncdf4 *(52)* (for working with environmental data in NetCDF formats), gstat *(53)* (for performing spatial interpolation/kriging), and lme4 *(54)* (for mixed model analyses).

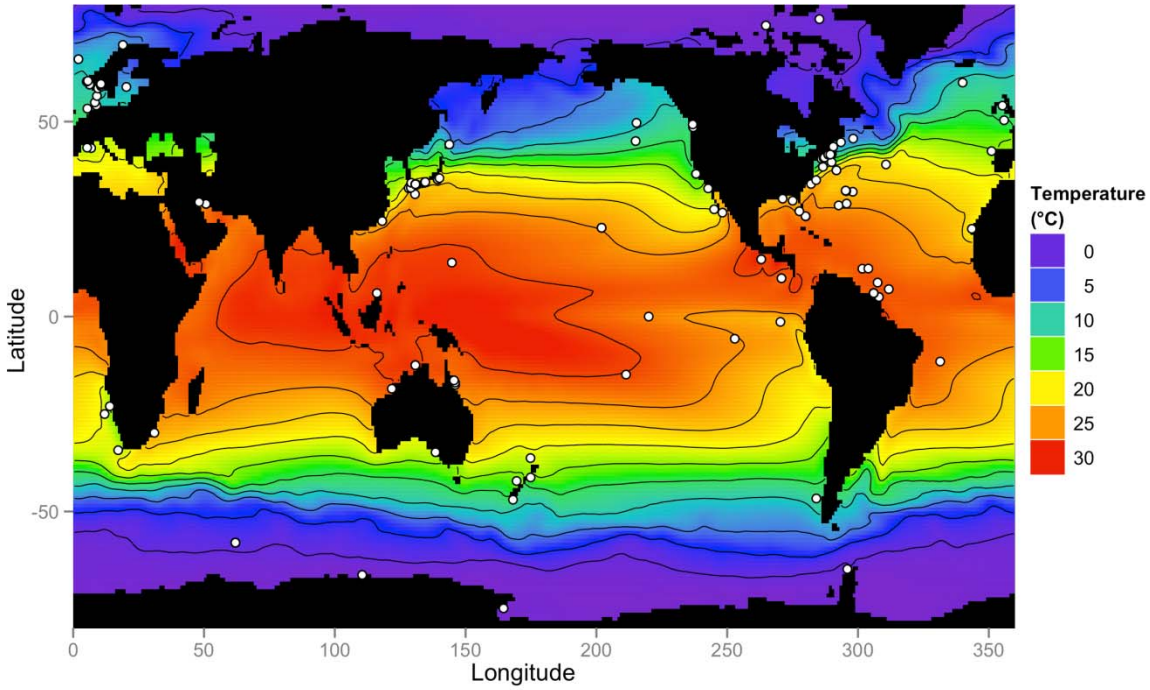

Fig. S1.

Mean annual temperatures across the oceans and the isolation locations of the 194 strains in our dataset, indicated by white dots. While most strains are isolated from coastal regions, we capture almost the entire temperature gradient, including the polar and tropical extremes.

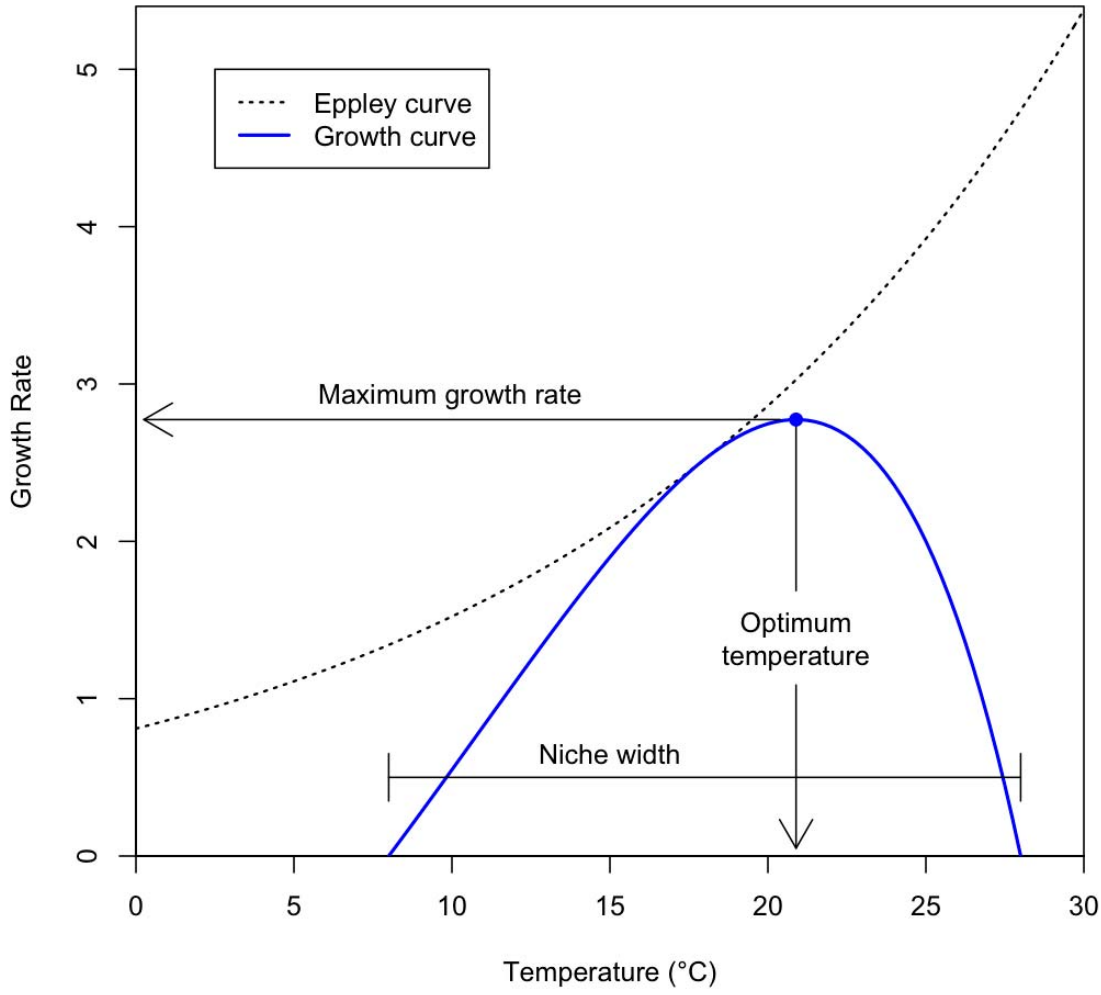

Fig. S2.

An example thermal tolerance curve, illustrating the skewness typical of all known ectotherms, including reptiles, amphibians, fish, algae, bacteria, and viruses. Niche width and the optimum temperature (at which the strain reaches its maximum growth rate) are shown. As in our model, this strain is bounded by the Eppley curve.

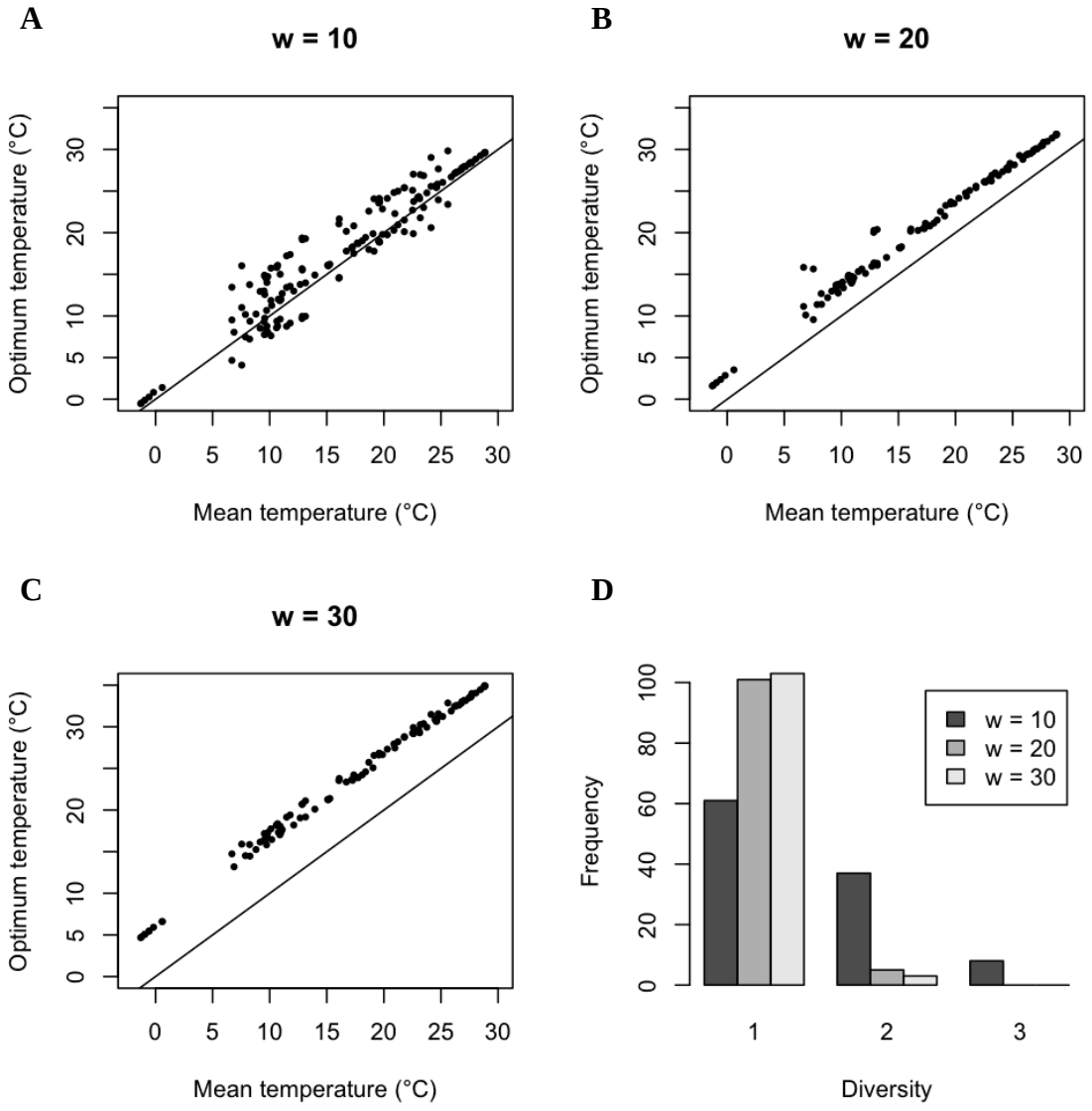

Fig. S3.

Eco-evolutionary model predictions of the evolutionarily stable optimum temperatures for growth given different niche widths (panels A-C; w = 10, 20, and 30°C, respectively). Also shown in D is the number of environments for which the equilibrium community consisted of 1, 2, or 3 coexisting strains, displayed for each of the various niche width assumptions. As niche width increases the frequency of obtaining multiple coexisting species declines.

A

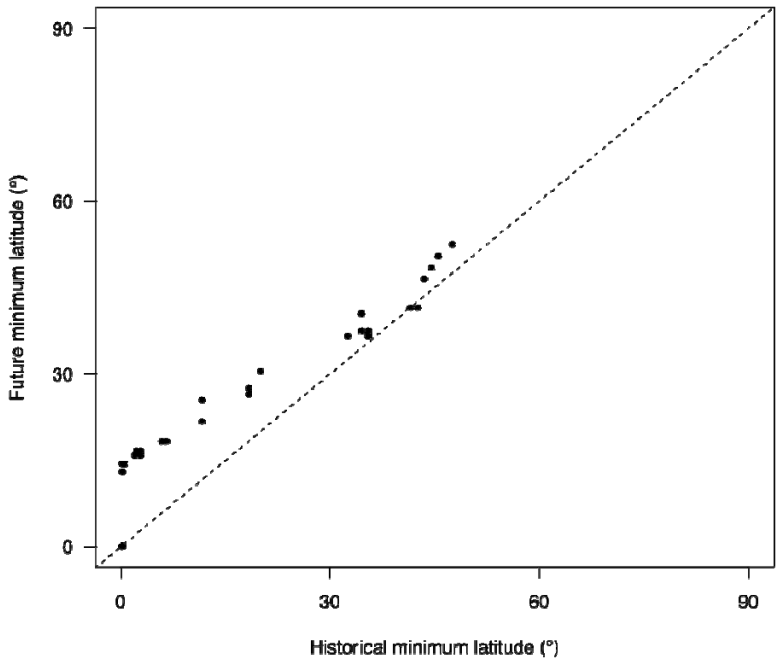

B

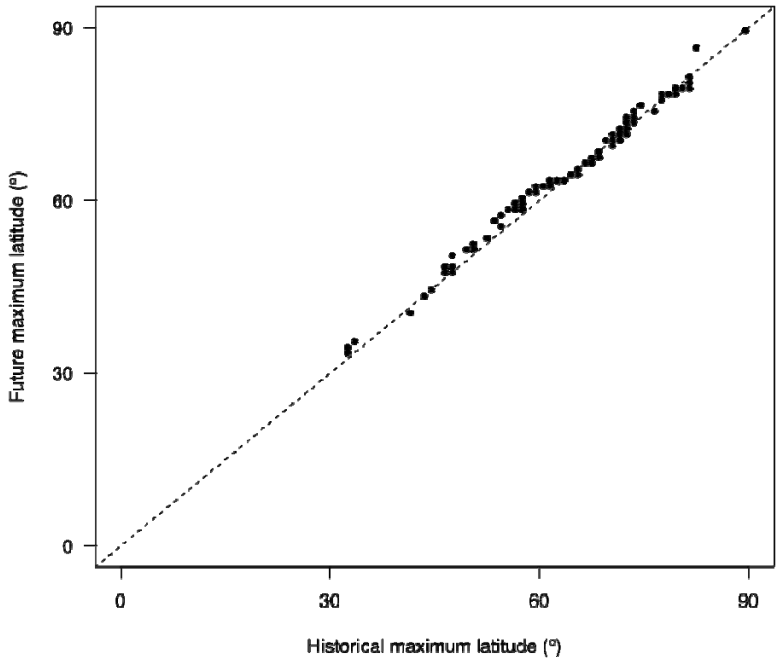

Fig. S4.

Predicted shifts in the A) equatorial and B) polar boundaries of all 194 strains. A) Points above the 1:1 dashed line have experienced a poleward shift in their lowest latitude at which they can grow. Almost all strains experience no change or poleward shifts. B) Points above the 1:1 dashed line have experienced a poleward shift in their highest latitude at which they can grow. Most strains experience a fairly small change in this latitude.

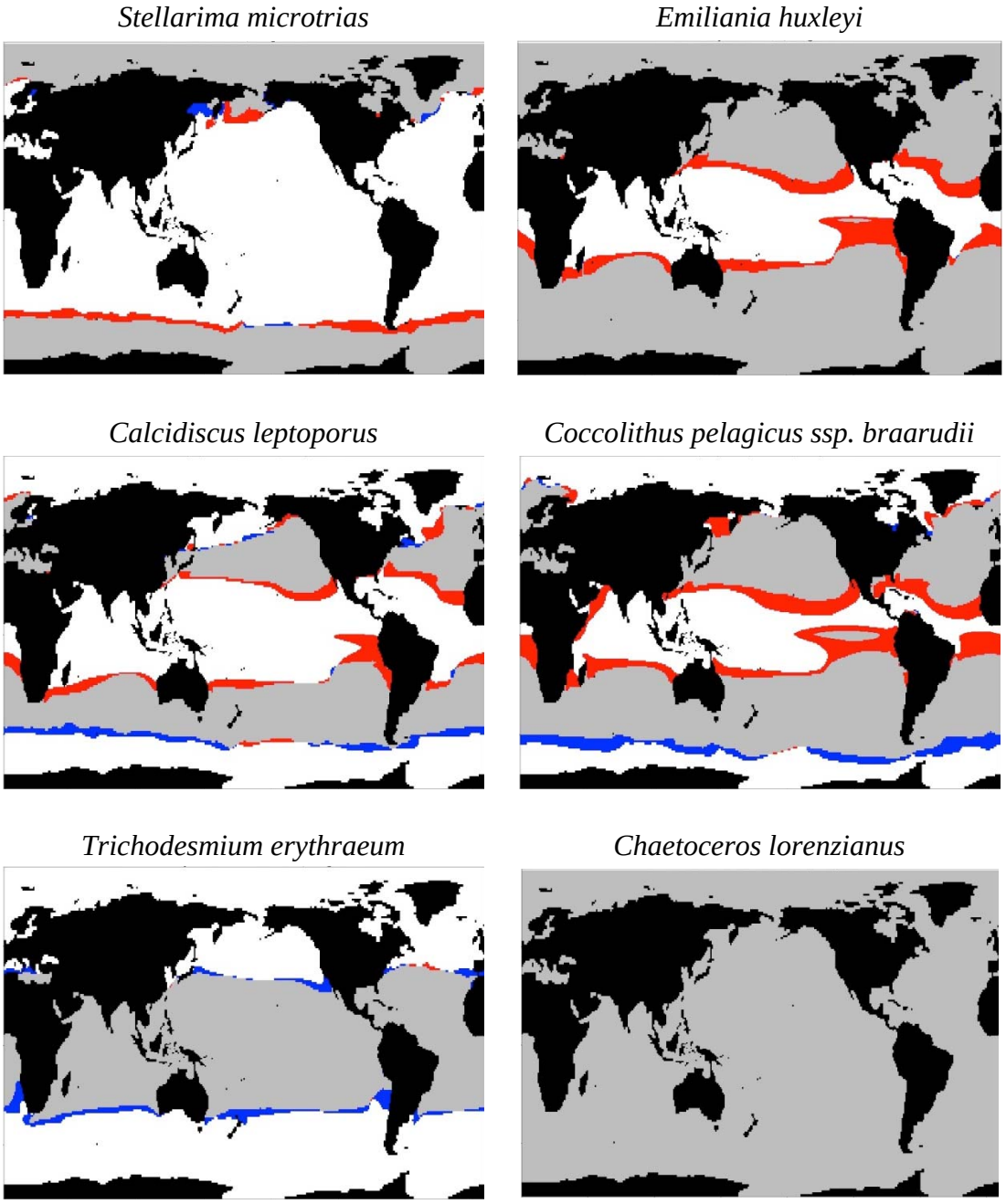

Fig. S5.

Examples of changes in the fundamental niche illustrating the diversity of ways individual strains may be affected. At each location a strain can persist (grey), be absent from the environment (white), or undergo range expansion (blue) or contraction (red) in the future. See figure S12 for the complete set of range maps.

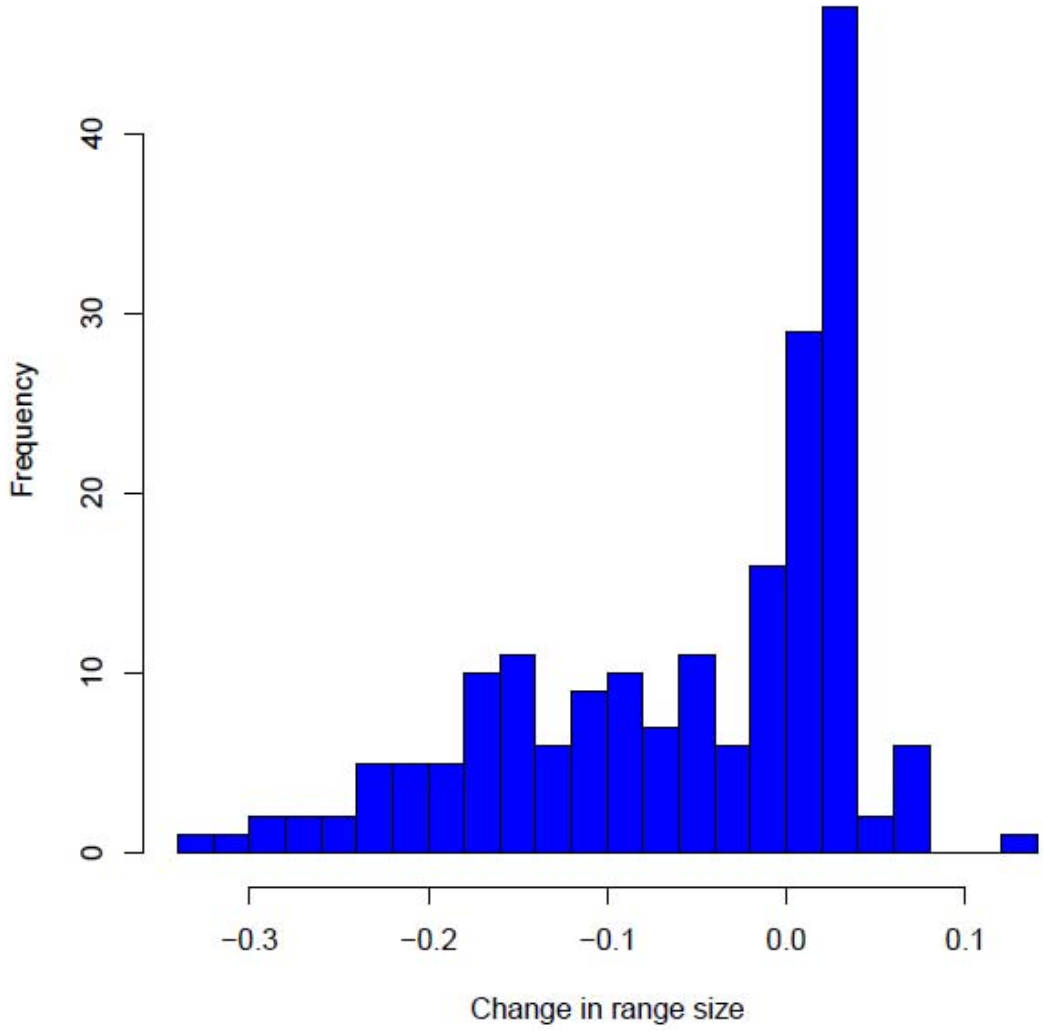

Fig. S6.

Histogram of per cent change in predicted strain range sizes. A number of strains experience a slight increase in their range, but a large number experience small to moderate decreases.

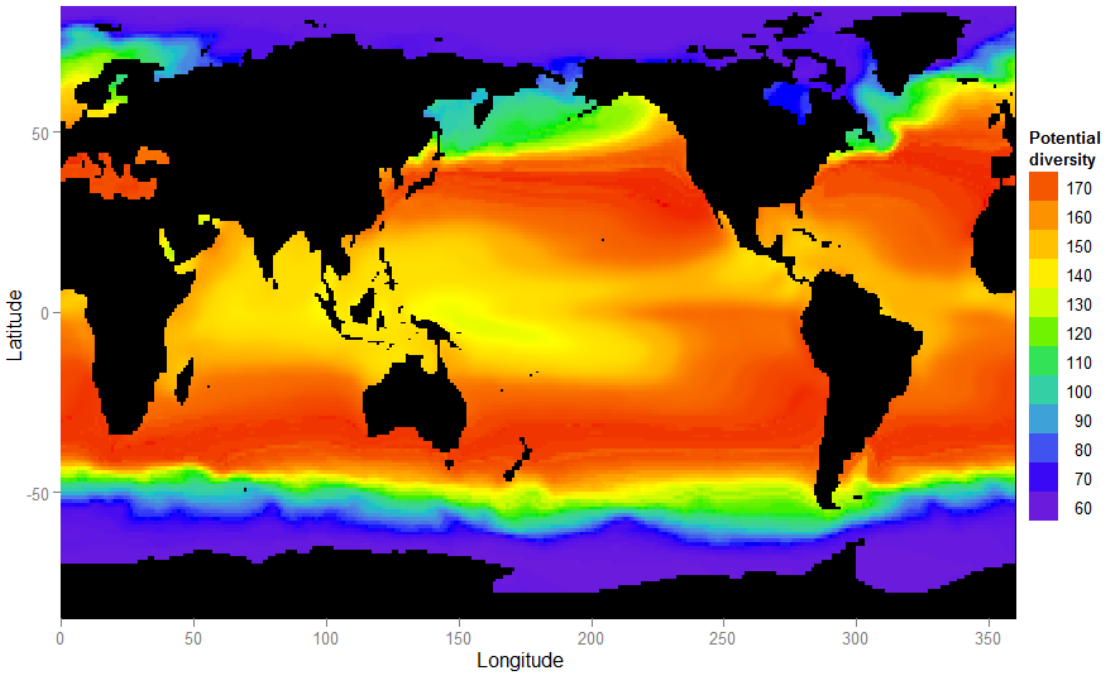

Fig. S7.

Potential diversity under past (1991-2000) temperature regimes. High diversity in temperate waters is a result of sampling bias, as most strains in our dataset were isolated in temperate waters, specifically off the US east coast, the European west coast and Japan.

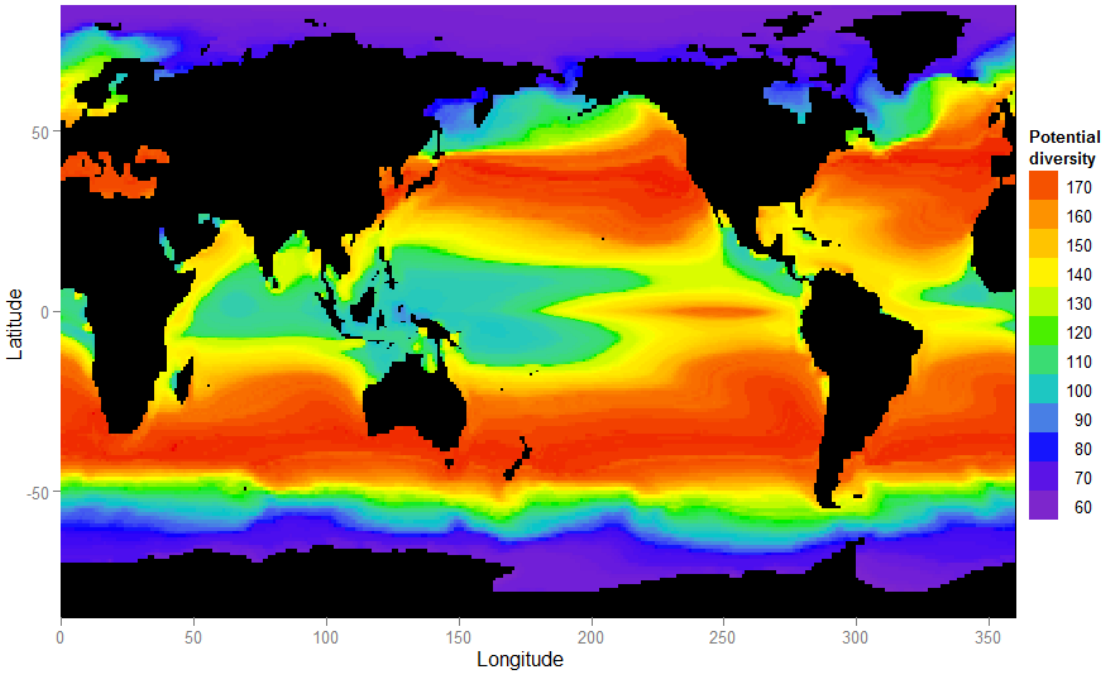

Fig. S8.

Potential diversity under future (2091-2100) temperature regimes. Temperature increase drives a large reduction in the potential diversity of the tropical Indian Ocean, Pacific Ocean and western Atlantic Ocean and an increase in the Antarctic Ocean.

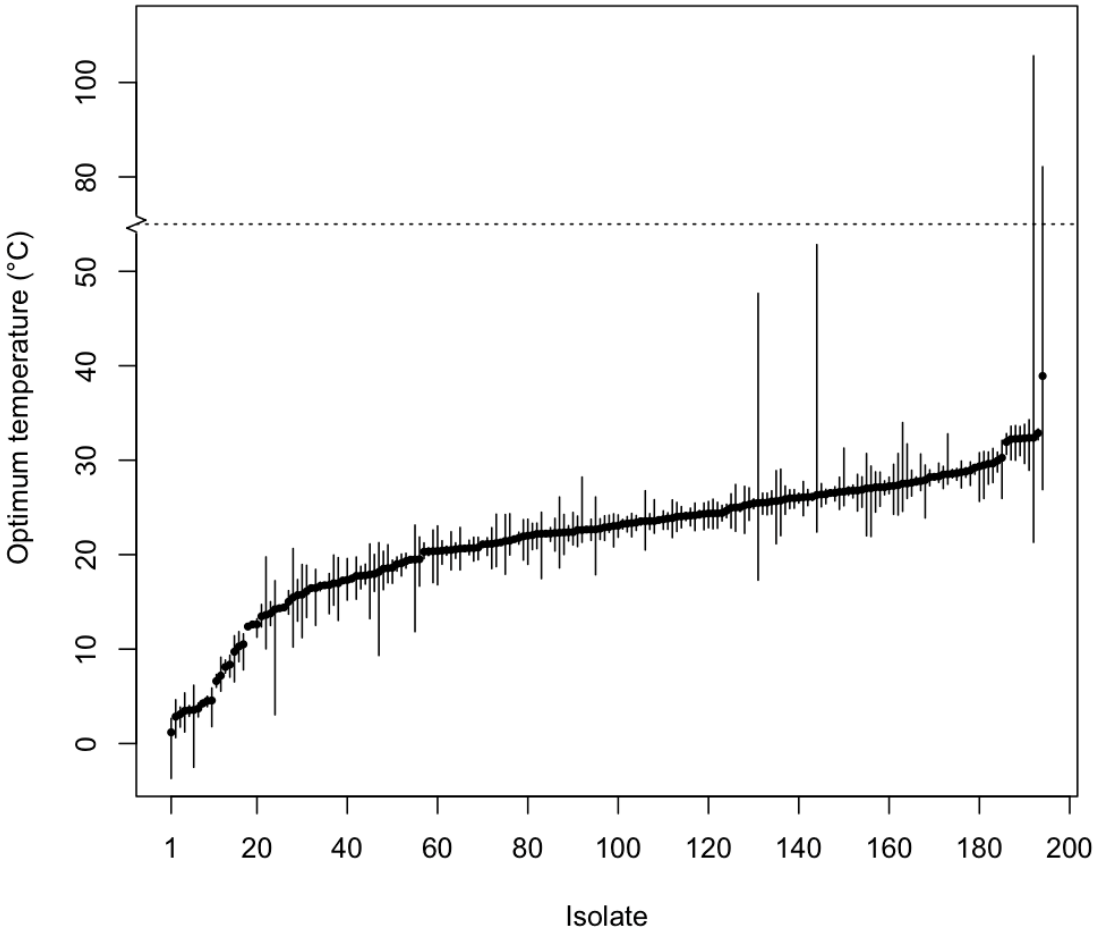

Fig. S9.

Estimates of uncertainty in optimum temperature for all strains, obtained through bootstrapping. Estimated optima are shown as points, while the 95% confidence intervals for the point estimates are shown by the error bars, obtained via our randomization analysis. Strains are ranked in ascending order of optimum temperature.

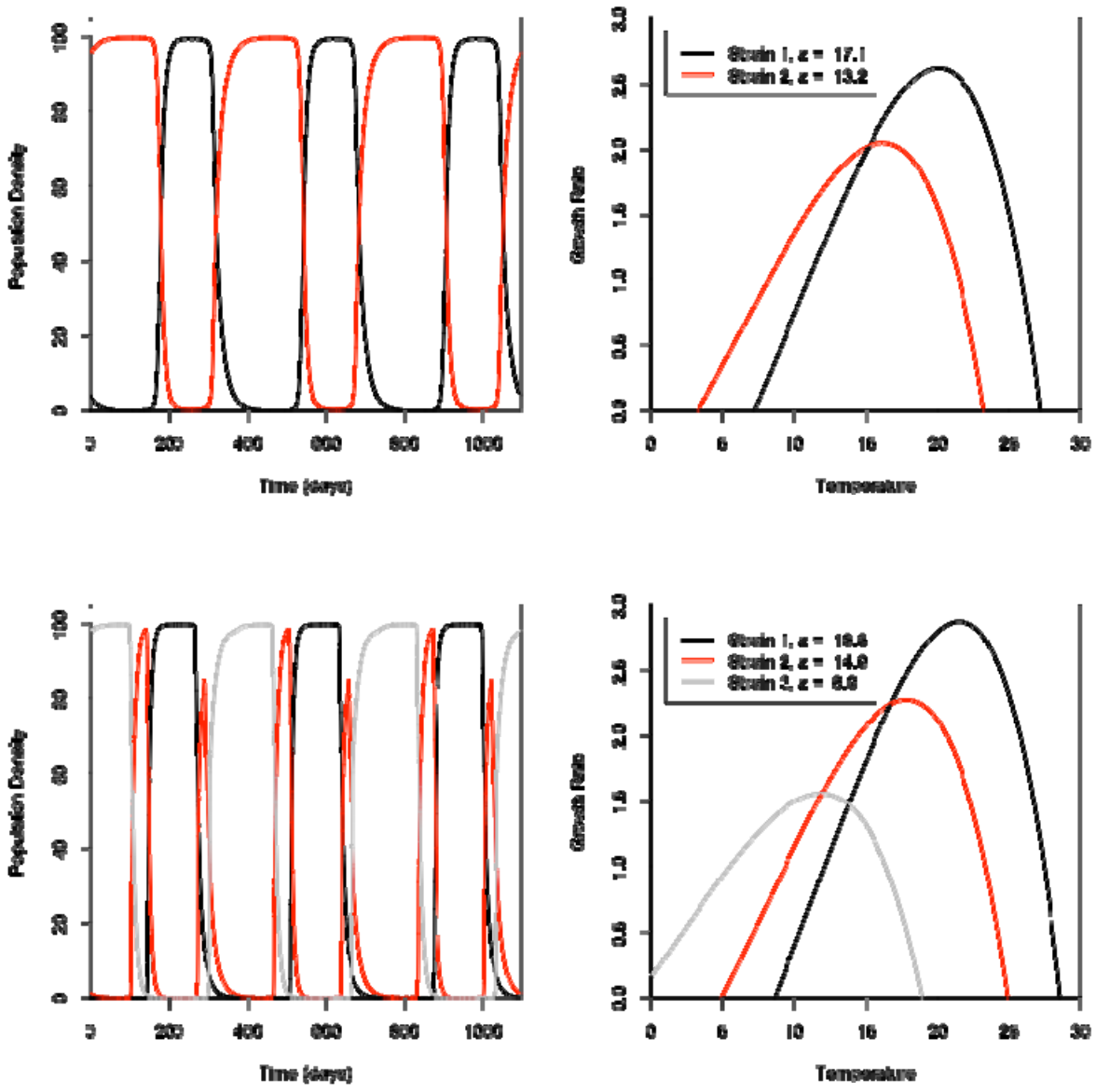

Fig. S10.

Example time series of population dynamics and corresponding species traits. The first row contains results for $w = 20$, while the second shows results for the same environment, but with a narrower niche width ($w = 10$) leading to three coexisting strains.

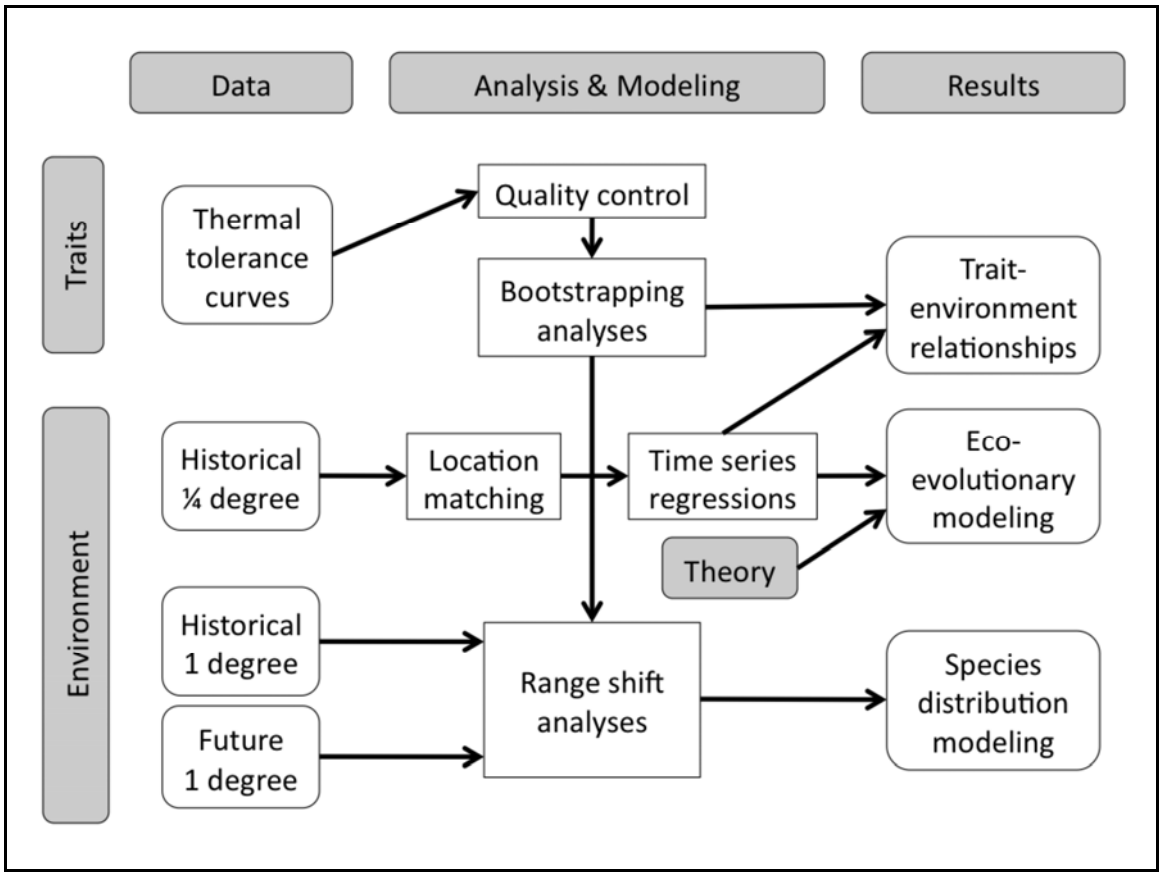

Fig. S11.
A schematic outlining all analyses and modeling performed.

Table S1.

Taxonomic model comparisons. Taxonomic levels are considered significant if their removal leads to an increase in AIC of >2 (i.e. dAIC < -2) relative to the full model, and are indicated here in boldface.

Trait	Model	AIC	dAIC
Optimum temperature for growth Full model: Mean temperature + (Mean temperature)^2 + Domain + Kingdom + Phylum + Class + Order + Family + Genus + Species + Strain	Full model	1091.407	0
	Full model - Domain	1089.407	2
	Full model - Kingdom	1090.960	0.447
	Full model - Phylum	1089.407	2
	Full model - Class	1089.407	2
	Full model - Order	1089.407	2
	Full model - Family	1089.407	2
	Full model - Genus	1092.006	-0.599
	Full model - Species	1098.854	**-7.447**
	Full model - Strain	1089.447	1.96
Temperature niche width Full model: Domain + Kingdom + Phylum + Class + Order + Family + Genus + Species + Strain	Full model	1522.816	0
	Full model - Domain	1521.898	0.918
	Full model - Kingdom	1520.816	2
	Full model - Phylum	1522.256	0.56
	Full model - Class	1520.816	2
	Full model - Order	1520.816	2
	Full model - Family	1520.816	2
	Full model - Genus	1521.336	1.48
	Full model - Species	1546.125	**-23.309**
	Full model - Strain	1520.816	2

Table S2.

A summary of the full models (as written in Table S1) used to test for a taxonomic signal. Significant random effects indicated in boldface.

Optimum temperature for growth		Temperature niche width	
Random effects			
Taxonomic level	*Variance explained*	*Taxonomic level*	*Variance explained*
Domain	<0.001	Domain	52.044
Kingdom	0.937	Kingdom	<0.001
Phylum	<0.001	Phylum	14.775
Class	<0.001	Class	<0.001
Order	<0.001	Order	<0.001
Family	<0.001	Family	<0.001
Genus	1.867	Genus	7.142
Species	**4.722**	Species	**55.514**
Strain	0.173	Strain	<0.001
Residual	8.868	Residual	91.489

Fixed effects

Term	*Estimate*	*Std. error*	*t-value*	*Term*	*Estimate*	*Std. error*	*t-value*
Intercept	7.216	1.141	6.326	Intercept	14.114	5.875	2.402
Mean temperature	1.358	0.133	10.238				
(Mean temperature)^2	-0.024	0.004	-5.657				

Table S3.
Eco-evolutionary model parameters.

	Symbol	Definition	Value or units
Resource variables	R	Available resource	Dynamic
	k	Half-saturation constant	1
	R_{in}	Total resource level	100
Biomass variables	N	Biomass	Dynamic; measured in resource units
	$m(T)$	Temperature dependent background mortality rate	Specific growth rate; $m = 0.5\left(ae^{bT}\right)$
	μ	Growth rate	Specific growth rate
	a	Eppley curve coefficient	0.81
	b	Eppley curve exponent	0.0631
	z_i	Competitive optima	°C
	w	Niche width	{10, 20, 30}, °C
Temperature variables	T	Temperature	°C
	τ	Period of temperature fluctuation	365 days
	ϕ	Minimum (maximum) temperature, if r is positive (negative)	°C
	r	Range of temperature fluctuation	°C
	α	Skewness of temperature fluctuation	Not applicable
	β	Temporal shift of temperature fluctuation	Days
Evolutionary parameters	ε	Evolution rate	0.01

Table S4.

Trait-environment models and associated Akaike weights.

Model	Average Akaike weight
Optimum ~ Mean	0.0153
Optimum ~ Range	0.0002
Optimum ~ Mean + Range	0.0313
Optimum ~ Mean + Mean^2	0.6661
Optimum ~ Mean + Mean^2 + Range	0.2871

Table S5 (separate file).
Phytoplankton temperature traits and data sources (citations 55-135).

Table S6 (separate file).
Phytoplankton growth rates and isolation locations, gathered from citations 55-135.

References and Notes

1. C. B. Field, M. J. Behrenfeld, J. T. Randerson, P. G. Falkowski, Primary production of the biosphere: integrating terrestrial and oceanic components. *Science* **281**, 237 (1998). doi:10.1126/science.281.5374.237 Medline

2. A. C. Redfield, The biological control of chemical factors in the environment. *Am. Sci.* **46**, 205 (1958).

3. P. G. Falkowski, R. T. Barber, V. Smetacek, Biogeochemical controls and feedbacks on ocean primary production. *Science* **281**, 200 (1998). doi:10.1126/science.281.5374.200 Medline

4. M. J. Behrenfeld *et al*., Climate-driven trends in contemporary ocean productivity. *Nature* **444**, 752 (2006). doi:10.1038/nature05317 Medline

5. D. G. Boyce, M. R. Lewis, B. Worm, Global phytoplankton decline over the past century. *Nature* **466**, 591 (2010). doi:10.1038/nature09268 Medline

6. M. Edwards, A. J. Richardson, Impact of climate change on marine pelagic phenology and trophic mismatch. *Nature* **430**, 881 (2004). doi:10.1038/nature02808 Medline

7. X. A. G. Morán, Á. López-Urrutia, A. Calvo-Díaz, W. K. W. Li, Increasing importance of small phytoplankton in a warmer ocean. *Glob. Change Biol.* **16**, 1137 (2010). doi:10.1111/j.1365-2486.2009.01960.x

8. L. Bopp *et al*., Potential impact of climate change on marine export production. *Global Biogeochem. Cycles* **15**, 81 (2001). doi:10.1029/1999GB001256

9. M. Steinacher *et al*., Projected 21st century decrease in marine productivity: A multi-model analysis. *Biogeosciences* **7**, 979 (2010). doi:10.5194/bg-7-979-2010

10. Materials and methods are available as supplementary materials on *Science* Online.

11. J. G. Kingsolver, The well-temperatured biologist. *Am. Nat.* **174**, 755 (2009). doi:10.1086/648310 Medline

12. R. W. Eppley, Temperature and phytoplankton growth in the sea. *Fish Bull.* **70**, 1063 (1972).

13. T. L. Martin, R. B. Huey, Why “suboptimal” is optimal: Jensen’s inequality and ectotherm thermal preferences. *Am. Nat.* **171**, E102 (2008). doi:10.1086/527502 Medline

14. J. Norberg, Biodiversity and ecosystem functioning: A complex adaptive systems approach. *Limnol. Oceanogr.* **49**, 1269 (2004). doi:10.4319/lo.2004.49.4_part_2.1269

15. S. A. H. Geritz, É. Kisdi, G. Meszéna, J. A. J. Metz, Evolutionarily singular strategies and the adaptive growth and branching of the evolutionary tree. *Evol. Ecol.* **12**, 35 (1997). doi:10.1023/A:1006554906681

16. P. A. Abrams, Modelling the adaptive dynamics of traits involved in inter- and intraspecific interactions: An assessment of three methods. *Ecol. Lett.* **4**, 166 (2001). doi:10.1046/j.1461-0248.2001.00199.x

17. J. C. Stegen, R. Ferriere, B. J. Enquist, Evolving ecological networks and the emergence of biodiversity patterns across temperature gradients. *Proc. Biol. Sci.* **279**, 1051 (2011). 10.1098/rspb.2011.1733 Medline

18. R. W. Reynolds *et al*., Daily high-resolution-blended analyses for sea surface temperature. *J. Clim.* **20**, 5473 (2007). doi:10.1175/2007JCLI1824.1

19. R. W. Reynolds, N. A. Rayner, T. M. Smith, D. C. Stokes, W. Wang, An improved in situ and satellite SST analysis for climate. *J. Clim.* **15**, 1609 (2002). doi:10.1175/1520-0442(2002)015<1609:AIISAS>2.0.CO;2

20. M. R. Kearney, W. Porter, Mechanistic niche modelling: combining physiological and spatial data to predict species' ranges. *Ecol. Lett.* **12**, 334 (2009). doi:10.1111/j.1461-0248.2008.01277.x Medline

21. I. P. C. C. Fourth Assessment Report, *IPCC, 2007: Climate Change 2007: The Physical Science Basis. Contribution of Working Group I to the Fourth Assessment Report of the Intergovernmental Panel on Climate Change [Solomon, S., D. Qin, M. Manning, Z. Chen, M. Marquis, K.B. Averyt, M. Tignor and* (Cambridge, United Kingdom and New York, NY, USA, 2007), p. 996.

22. N. Nakicenovic *et al.*, *Special report on emissions scenarios: A special report of Working Group III of the Intergovernmental Panel on Climate Change* N. Nakićenović, R. Swart, Eds. (Cambridge University Press, Cambridge, UK, 2000; http://www.osti.gov/energycitations/product.biblio.jsp?osti_id = 15009867), p. 595.

23. T. Delworth *et al*., GFDL's CM2 global coupled climate models. Part I: Formulation and simulation characteristics. *J. Clim.* **19**, 643 (2006). doi:10.1175/JCLI3629.1

24. D. W. McKenney, J. H. Pedlar, K. Lawrence, K. Campbell, M. F. Hutchinson, Potential impacts of climate change on the distribution of North American trees. *Bioscience* **57**, 939 (2007). doi:10.1641/B571106

25. D. U. Hooper *et al*., A global synthesis reveals biodiversity loss as a major driver of ecosystem change. *Nature* **486**, 105 (2012). Medline

26. D. Tilman, D. Wedin, J. Knops, Productivity and sustainability influenced by biodiversity in grassland ecosystems. *Nature* **379**, 718 (1996). doi:10.1038/379718a0

27. P. B. Reich *et al*., Impacts of biodiversity loss escalate through time as redundancy fades. *Science* **336**, 589 (2012). doi:10.1126/science.1217909 Medline

28. C. A. Deutsch *et al*., Impacts of climate warming on terrestrial ectotherms across latitude. *Proc. Natl. Acad. Sci. U.S.A.* **105**, 6668 (2008). doi:10.1073/pnas.0709472105 Medline

29. K. Härnström, M. Ellegaard, T. J. Andersen, A. Godhe, Hundred years of genetic structure in a sediment revived diatom population. *Proc. Natl. Acad. Sci. U.S.A.* **108**, 4252 (2011). doi:10.1073/pnas.1013528108 Medline

30. A. F. Bennett, R. E. Lenski, in *In the Light of Evolution. Volume 1. Adaptation and Complex Design*, J. C. Avise, F. J. Ayala, Eds. (National Academies Press, 2007), pp. 225–238.

31. J. L. Knies, R. Izem, K. L. Supler, J. G. Kingsolver, C. L. Burch, The genetic basis of thermal reaction norm evolution in lab and natural phage populations. *PLoS Biol.* **4**, e201 (2006). doi:10.1371/journal.pbio.0040201 Medline

32. I. E. Huertas, M. Rouco, V. López-Rodas, E. Costas, Warming will affect phytoplankton differently: evidence through a mechanistic approach. *Proc. Biol. Sci.* **278**, 3534 (2011). doi:10.1098/rspb.2011.0160 Medline

33. S. L. Chown *et al*., Adapting to climate change: A perspective from evolutionary physiology. *Clim. Res.* **43**, 3 (2010). doi:10.3354/cr00879

34. M. J. Angilletta Jr., R. S. Wilson, C. A. Navas, R. S. James, Tradeoffs and the evolution of thermal reaction norms. *Trends Ecol. Evol.* **18**, 234 (2003). doi:10.1016/S0169-5347(03)00087-9

35. J. Frantz, P. Novak, g3data (2000) (available at http://www.frantz.fi/software/g3data.php).

36. A. Gelman, J. Hill, *Data Analysis Using Regression and Multilevel/Hierachical Models* (Cambridge University Press, Cambridge, UK, 2007), p. 624.

37. K. P. Burnham, D. R. Anderson, *Model Selection and Multimodel Inference: A Practical Information-Theoretic Approach* (Springer-Verlag, New York, ed. 2nd, 2002), p. 488.

38. A. S. Schwaderer *et al*., Eco-evolutionary differences in light utilization traits and distributions of freshwater phytoplankton. *Limnol. Oceanogr.* **56**, 589 (2011). doi:10.4319/lo.2011.56.2.0589

39. A. J. Kerkhoff, W. F. Fagan, J. J. Elser, B. J. Enquist, Phylogenetic and growth form variation in the scaling of nitrogen and phosphorus in the seed plants. *Am. Nat.* **168**, E103 (2006). doi:10.1086/507879 Medline

40. M. D. Guiry, G. M. Guiry, AlgaeBaseWorld-wide electronic publication, National University of Ireland, Galway (2012) (available at http://www.algaebase.org).

41. ITIS, Integrated Taxonomic Information System, (2012) (available at http://www.itis.gov).

42. J. E. Bissinger, D. J. S. Montagnes, J. Sharples, D. Atkinson, Predicting marine phytoplankton maximum growth rates from temperature: Improving on the Eppley curve using quantile regression. *Limnol. Oceanogr.* **53**, 487 (2008). doi:10.4319/lo.2008.53.2.0487

43. R. Lande, Natural selection and random genetic drift in phenotypic evolution. *Evolution* **30**, 314 (1976). doi:10.2307/2407703

44. C. J. E. Metcalf *et al*., Evolution of flowering decisions in a stochastic, density-dependent environment. *Proc. Natl. Acad. Sci. U.S.A.* **105**, 10466 (2008). doi:10.1073/pnas.0800777105 Medline

45. D. Z. Childs, T. N. Coulson, J. M. Pemberton, T. H. Clutton-Brock, M. Rees, Predicting trait values and measuring selection in complex life histories: reproductive allocation decisions in Soay sheep. *Ecol. Lett.* **14**, 985 (2011). doi:10.1111/j.1461-0248.2011.01657.x Medline

46. P. A. Abrams, ‘Adaptive Dynamics’ vs. ‘adaptive dynamics’. *J. Evol. Biol.* **18**, 1162 (2005). doi:10.1111/j.1420-9101.2004.00843.x Medline

47. S. M. Griffies *et al*., Formulation of an ocean model for global climate simulations. *Ocean Science* **1**, 45 (2005). doi:10.5194/os-1-45-2005

48. R Core Team, (2012). R: A language and environment for statistical computing. R Foundation for Statistical Computing, Vienna, Austria. ISBN 3-900051-07-0, URL http://www.R-project.org/.

49. B. Bolker and R Development Core Team (2012). bbmle: Tools for general maximum likelihood estimation. R package version 1.0.5.2. http://CRAN.R-project.org/package = bbmle

50. H. Wickham, Reshaping data with the reshape package. *J. Stat. Softw.* **21**, 12 (2007).

51. H. Wickham, ggplot2: elegant graphics for data analysis. Springer New York (2009).

52. D. Pierce, ncdf4: Interface to Unidata netCDF (version 4 or earlier) format data files. R package version 1.0 (2010) (available at http://cran.r-project.org/package = ncdf4).

53. E. J. Pebesma, Multivariable geostatistics in S: the gstat package. *Comput. Geosci.* **30**, 683 (2004). doi:10.1016/j.cageo.2004.03.012

54. D. Bates, M. Maechler, B. Bolker, lme4: Linear mixed-effects models using S4 classes. R package version 0.999375-42 (2011). http://cran.r-project.org/package = lme4.

55. V. Vona *et al*., Temperature responses of growth, photosynthesis, respiration and NADH: Nitrate reductase in cryophilic and mesophilic algae. *New Phytol.* **163**, 325 (2004). doi:10.1111/j.1469-8137.2004.01098.x

56. M.-L. Teoh, W.-L. Chu, H. Marchant, S.-M. Phang, Influence of culture temperature on the growth, biochemical composition and fatty acid profiles of six Antarctic microalgae. *J. Appl. Phycol.* **2**, 421 (2005).

57. X. Wang, K. W. Tang, Y. Wang, W. O. Smith, Jr., Temperature effects on growth, colony development and carbon partitioning in three Phaeocystis species. *Aquat. Biol.* **9**, 239 (2010). doi:10.3354/ab00256

58. M. Fiala, L. Oriol, Light-temperature interactions on the growth of Antarctic diatoms. *Polar Biol.* **10**, 629 (1990). doi:10.1007/BF00239374

59. G. Jacques, Some ecophysiological aspects of the Antarctic phytoplankton. *Polar Biol.* **2**, 27 (1983). doi:10.1007/BF00258282

60. L. Rhodes, B. Peake, A. L. MacKenzie, S. Marwick, Coccolithophores Gephyrocapsa oceanica and Emiliania huxleyi (Prymnesiophyceae = Haptophyceae) in New Zealand's coastal waters: Characteristics of blooms and growth in laboratory culture. *N. Z. J. Mar. Freshw. Res.* **29**, 345 (1995). doi:10.1080/00288330.1995.9516669

61. E. T. Buitenhuis, T. Pangerc, D. J. Franklin, C. Le Quéré, G. Malin, Growth rates of six coccolithophorid strains as a function of temperature. *Limnol. Oceanogr.* **53**, 1181 (2008). doi:10.4319/lo.2008.53.3.1181

62. M. K. de Boer, E. M. Koolmees, E. G. Vrieling, A. M. Breeman, M. van Rijssel, Temperature responses of three Fibrocapsa japonica strains (Raphidophyceae) from different climate regions. *J. Plankton Res.* **27**, 47 (2005). doi:10.1093/plankt/fbh149

63. M. H. Conte, A. Thompson, D. Lesley, R. P. Harris, Genetic and physiological influences on the alkenone/alkenoate versus growth temperature relationship in Emiliania huxleyi and

Gephyrocapsa oceanica. *Geochim. Cosmochim. Acta* **62**, 51 (1998). doi:10.1016/S0016-7037(97)00327-X

64. J. A. Cannon, in *Toxic Phytoplankton Blooms in the Sea*, T. J. Smayda, Y. Shimizu, Eds. (Elsevier Science, 1993), pp. 741–745.

65. S. M. Renaud, H. C. Zhou, D. L. Parry, L.-V. Thinh, K. C. Woo, Effect of temperature on the growth, total lipid content and fatty acid composition of recently isolated tropical microalgae Isochrysis sp., Nitzschia closterium, Nitzschia paleacea, and commercial species Isochrysis sp. (clone T. ISO). *J. Appl. Phycol.* **7**, 595 (1995). doi:10.1007/BF00003948

66. S. M. Renaud, L.-V. Thinh, G. Lambrinidis, D. L. Parry, Effect of temperature on growth, chemical composition and fatty acid composition of tropical Australian microalgae grown in batch cultures. *Aquaculture* **211**, 195 (2002). doi:10.1016/S0044-8486(01)00875-4

67. P. D. Chappell, E. A. Webb, A molecular assessment of the iron stress response in the two phylogenetic clades of Trichodesmium. *Environ. Microbiol.* **12**, 13 (2010). doi:10.1111/j.1462-2920.2009.02026.x Medline

68. K. J. S. Meier, C. Höll, H. Willems, Effect of temperature on culture growth and cyst production in the calcareous dinoflagellates Calciodinellum albatrosianum, Leonella granifera and Pernambugia tuberosa. *Micropaleontology* **50**, (Suppl_1), 93 (2004). doi:10.2113/50.Suppl_1.93

69. E. M. Hulburt, R. R. L. Guillard, The relationship of the distribution of the diatom Skeletonema tropicum to temperature. *Ecology* **49**, 337 (1968). doi:10.2307/1934464

70. E. M. Hulburt, The adaptation of marine phytoplankton species to nutrient and temperature. *Ocean Science and Engineering* **7**, 187 (1982).

71. G. Usup, D. M. Kulis, D. M. Anderson, Growth and toxin production of the toxic dinoflagellate Pyrodinium bahamense var. compressum in laboratory cultures. *Nat. Toxins* **2**, 254 (1994). doi:10.1002/nt.2620020503 Medline

72. W. H. Thomas, Effects of temperature and illuminance on cell division rates of three species of tropical oceanic phytoplankton. *J. Phycol.* **2**, 17 (1966). doi:10.1111/j.1529-8817.1966.tb04586.x

73. L. I. Falcón, S. Pluvinage, E. J. Carpenter, Growth kinetics of marine unicellular N2-fixing cyanobacterial isolates in continuous culture in relation to phosphorus and temperature. *Mar. Ecol. Prog. Ser.* **285**, 3 (2005). doi:10.3354/meps285003

74. H. K. Schöne, The influence of light and temperature on the growth rates of six phytoplankton species from the upwelling area off Northwest Africa. *Rapports et Procés-verbaux des Réunions* **180**, 246 (1982).

75. T. G. Chin, C. F. Chen, S. C. Liu, S. S. Wu, Influence of temperature and salinity on the growth of three species of planktonic diatoms. *Oceanol. Limnol. Sin.* **7**, 373 (1965).

76. J. Bollmann, C. Klaas, L. E. Brand, Morphological and physiological characteristics of Gephyrocapsa oceanica var. typica Kamptner 1943 in culture experiments: evidence for genotypic variability. *Protist* **161**, 78 (2010). doi:10.1016/j.protis.2009.08.002 Medline

77. C. J. Band-Schmidt, Effects of growth medium, temperature, salinity and seawater source on the growth of Gymnodinium catenatum (Dinophyceae) from Bahia Concepcion, Gulf of California, Mexico. *J. Plankton Res.* **26**, 1459 (2004). doi:10.1093/plankt/fbh133

78. L. McKay, D. Kamykowski, E. Milligan, B. Schaeffer, G. Sinclair, Comparison of swimming speed and photophysiological responses to different external conditions among three Karenia brevis strains. *Harmful Algae* **5**, 623 (2006). doi:10.1016/j.hal.2005.12.001

79. R. W. Krawiec, Autecology and clonal variability of the marine centric diatom Thalassiosira rotula (Bacillariophyceae) in response to light, temperature and salinity. *Mar. Biol.* **69**, 79 (1982). doi:10.1007/BF00396964

80. L. R. Moore, R. Goericke, S. W. Chisholm, Comparative physiology of Synechococcus and Prochlorococcus: Influence of light and temperature on growth, pigments, fluorescence and absorptive properties. *Mar. Ecol. Prog. Ser.* **116**, 259 (1995). doi:10.3354/meps116259

81. C. M. James, S. Al-Hinty, A. E. Salman, Growth and ω3 fatty acid and amino acid composition of microalgae under different temperature regimes. *Aquaculture* **77**, 337 (1989). doi:10.1016/0044-8486(89)90218-4

82. S. Kahn, O. Arakawa, Y. Onoue, Physiological investigations of a neurotoxin-producing phytoflagellate, Chattonella marina (Raphidophyceae). *Aquacult. Res.* **29**, 9 (1998).

83. N. Watabe, K. M. Wilbur, Effects of temperature on growth, calcification, and coccolith form in Coccolithus huxleyi. *Limnol. Oceanogr.* **11**, 567 (1966). doi:10.4319/lo.1966.11.4.0567

84. W. S. Maddux, R. F. Jones, Some interactions of temperature, light intensity, and nutrient concentration during the continuous culture of Nitzschia closterium and Tetraselmis sp. *Limnol. Oceanogr.* **9**, 79 (1964). doi:10.4319/lo.1964.9.1.0079

85. W. H. Thomas, A. N. Dodson, C. A. Linden, Optimum light and temperature requirements for Gymnodinium splendens, a larval fish food organism. *Fish Bull.* **71**, 599 (1973).

86. T. Yamatogi, M. Sakaguti, N. Takagi, M. Iwataki, K. Matsuoka, Effects of temperature, salinity and light intensity on the growth of a harmful dinoflagellate Cochlodinium polykrikoides Margalef occurring in coast waters of West Kyushu, Japan. *Bull. Plankton Soc. Japan* **52**, 4 (2005).

87. M. Yamaguchi, T. Honjo, Effects of temperature, salinity and irradiance on the growth of the noxious red tide flagellate Gymnodinium nagasakiense (Dinophyceae). *Nippon Suisan Gakkai Shi* **55**, 2029 (1989). doi:10.2331/suisan.55.2029

88. R. L. Miller, D. L. Kamykowski, Effects of temperature, salinity, irradiance and diurnal periodicity on growth and photosynthesis in the diatom Nitzschia americana: Light-saturated growth. *J. Phycol.* **22**, 339 (1986). doi:10.1111/j.1529-8817.1986.tb00033.x

89. Y. Nakamura, M. M. Watanabe, Growth characteristics of Chattonella antiqua (Raphidophyceae). *J. Oceanogr. Soc. Jpn* **39**, 110 (1983). doi:10.1007/BF02070796

90. T. Nishikawa, M. Yamaguchi, Effect of temperature on light-limited growth of the harmful diatom Eucampia zodiacus Ehrenberg, a causative organism in the discoloration of Porphyra thalli. *Harmful Algae* **5**, 141 (2006). doi:10.1016/j.hal.2005.06.007

91. K. Ono, S. Khan, Y. Onoue, Effects of temperature and light intensity on the growth and toxicity of Heterosigma akashiwo (Raphidophyceae). *Aquacult. Res.* **31**, 427 (2000). doi:10.1046/j.1365-2109.2000.00463.x

92. E. Breitbarth, A. Oschlies, J. LaRoche, Physiological constraints on the global distribution of Trichodesmium – effect of temperature on diazotrophy. *Biogeosciences* **4**, 53 (2007). doi:10.5194/bg-4-53-2007

93. S. H. Baek, S. Shimode, T. Kikuchi, Growth of dinoflagellates, Ceratium furca and Ceratium fusus in Sagami Bay, Japan: The role of temperature, light intensity and photoperiod. *Harmful Algae* **7**, 163 (2008). doi:10.1016/j.hal.2007.06.006

94. Y. Suzuki, M. Takahashi, Growth responses of several diatom species isolated from various environments to temperature. *J. Phycol.* **31**, 880 (1995). doi:10.1111/j.0022-3646.1995.00880.x

95. H. A. Barker, The culture and physiology of the marine dinoflagellates. *Arch. Mikrobiol.* **6**, 157 (1935). doi:10.1007/BF00407285

96. R. R. L. Guillard, J. H. Ryther, Studies of marine planktonic diatoms. I. Cyclotella nana Hustedt, and Detonula confervacea (cleve) Gran. *Can. J. Microbiol.* **8**, 229 (1962). doi:10.1139/m62-029 Medline

97. J. H. Ryther, The ecology of phytoplankton blooms in Moriches Bay and Great South Bay, Long Island, New York. *Biol. Bull.* **106**, 198 (1954). doi:10.2307/1538713

98. P. A. Thompson, M.-X. Guo, P. J. Harrison, Effects of variation in temperature. I. On the biochemical composition of eight species of marine phytoplankton. *J. Phycol.* **28**, 481 (1992). doi:10.1111/j.0022-3646.1992.00481.x

99. H. Curl Jr., G. C. McLeod, The physiological ecology of a marine diatom, Skeletonema costatum (Grev.) Cleve. *J. Mar. Res.* **19**, 70 (1961).

100. D. Karentz, T. J. Smayda, Temperature and seasonal occurrence patterns of 30 dominant phytoplankton species in Narragansett Bay over a 22-year period (1959-1980). *Mar. Ecol. Prog. Ser.* **18**, 277 (1984). doi:10.3354/meps018277

101. T. J. Smayda, Experimental observations on the influence of temperature, light, and salinity on cell division of the marine diatom, Detonula confervacea (Cleve) Gran. *J. Phycol.* **5**, 150 (1969). doi:10.1111/j.1529-8817.1969.tb02596.x

102. C. R. Tomas, Olisthodiscus luteus (Chrysophyceae) I. Effects of salinity and temperature on growth, motillty and survival. *J. Phycol.* **14**, 309 (1978). doi:10.1111/j.1529-8817.1978.tb00303.x

103. L. Ignatiades, T. J. Smayda, Autecological studies on the marine diatom Rhizosolenia fragilissima Bergon. I. The influence of light, temperature, and salinity. *J. Phycol.* **6**, 332 (1970).

104. P. G. Falkowski, The adenylate energy charge in marine phytoplantkon: The effect of temperature on the physiological state of Skeletonema costatum (Grev.) Cleve. *J. Exp. Mar. Biol. Ecol.* **27**, 37 (1977). doi:10.1016/0022-0981(77)90052-1

105. E. G. Durbin, Studies on the autecology of the marine diatom Thalassiosira nordenskioldii Cleve. I. The influence of daylength, light intensity, and temperature on growth. *J. Phycol.* **10**, 220 (1974).

106. M. W. Fawley, Effects of light intensity and temperature interactions on growth characteristics of Phaeodactylum tricornutum (Bacillariophyceae). *J. Phycol.* **20**, 67 (1984). doi:10.1111/j.0022-3646.1984.00067.x

107. C. J. Watras, S. W. Chisholm, D. M. Anderson, Regulation of growth in an estuarine clone of Gonyaulax tamarensis Lebour: Salinity-dependent temperature responses. *J. Exp. Mar. Biol. Ecol.* **62**, 25 (1982). doi:10.1016/0022-0981(82)90214-3

108. I. Bravo, D. M. Anderson, The effects of temperature, growth medium and darkness on excystment and growth of the toxic dinoflagellate Gymnodinium catenatum from northwest Spain. *J. Plankton Res.* **16**, 513 (1994). doi:10.1093/plankt/16.5.513

109. D. Grzebyk, B. Berland, Influences of temperature, salinity and irradiance on growth of Prorocentrum minimum (Dinophyceae) from the Mediterranean Sea. *J. Plankton Res.* **18**, 1837 (1996). doi:10.1093/plankt/18.10.1837m

110. S. M. Etheridge, C. S. Roesler, Effects of temperature, irradiance, and salinity on photosynthesis, growth rates, total toxicity, and toxin composition for Alexandrium fundyense isolates from the Gulf of Maine and Bay of Fundy. *Deep Sea Res. Part II Top. Stud. Oceanogr.* **52**, 2491 (2005). doi:10.1016/j.dsr2.2005.06.026

111. R. El-Sabaawi, P. J. Harrison, Interactive effects of irradiance and temperature on the photosynthetic physiology of the pennate diatom Pseudo-nitzschia granii (Bacillariophyceae) from the northeast subarctic Pacific. *J. Phycol.* **42**, 778 (2006). doi:10.1111/j.1529-8817.2006.00246.x

112. N. I. Lewis, S. S. Bates, J. L. McLachlan, J. C. Smith, in *Toxic Phytoplankton Blooms in the Sea*, T. J. Smayda, Y. Shimizu, Eds. (Elsevier Science, 1993), pp. 601–606.

113. G. Kräbs, C. Büchel, Temperature and salinity tolerances of geographically separated Phaeodactylum tricornutum Böhlin strains: maximum quantum yield of primary photochemistry, pigmentation, proline content and growth. *Bot. Mar.* **54**, 231 (2011). doi:10.1515/bot.2011.037

114. A. M. Johnston, The effect of environmental variables on 13C discrimination by two marine phytoplankton. *Mar. Ecol. Prog. Ser.* **132**, 257 (1996). doi:10.3354/meps132257

115. S. Khan, O. Arakawa, Y. Onoue, Growth characteristics of a neurotoxin-producing chloromonad Fibrocapsa japonica (Raphidophyceae). *J. World Aquacult. Soc.* **27**, 247 (1996). doi:10.1111/j.1749-7345.1996.tb00606.x

116. L. A. Hobson, Effects of interactions of irradiance, daylength, and temperature on division rates of three species of marine unicellular algae. *J. Fish. Res. Board Can.* **31**, 391 (1974). doi:10.1139/f74-066

117. N. Grimm, T. Weisse, Die temperaturabhängigkeit des wachstums von Phaeocystis pouchetii (Haptophyceae) in batchkulturen. *Helgol. Meersunters.* **39**, 201 (1985). doi:10.1007/BF01997450

118. M. Ø. Jensen, Ø. Moestrup, Autecology of the toxic dinoflagellate Alexandrium ostenfeldii: Life history and growth at different temperatures and salinities. *Eur. J. Phycol.* **32**, 9 (1997). doi:10.1080/09541449710001719325

119. B. Edvardsen, E. Paasche, Two motile stages of Chrysochromulina polylepis (Prymnesiophyceae): Morphology, growth and toxicity. *J. Phycol.* **28**, 104 (1992). doi:10.1111/j.0022-3646.1992.00104.x

120. A. M. Sundström *et al*., Gymnodinium corollarium sp. nov. (Dinophyceae) - A new cold-water dinoflagellate responsible for cyst sedimentation events in the Baltic Sea. *J. Phycol.* **45**, 938 (2009). doi:10.1111/j.1529-8817.2009.00712.x

121. J. Throndsen, Occurrence and productivity of small marine flagellates. *Nord. J. Bot.* **23**, 269 (1976).

122. M. V. Nielsen, Growth and chemical composition of the toxic dinoflagellate Gymnodinium galatheanum in relation to irradiance, temperature and salinity. *Mar. Ecol. Prog. Ser.* **136**, 205 (1996). doi:10.3354/meps136205

123. M. V. Nielsen, C. P. Tønseth, Temperature and salinity effect on growth and chemical composition of Gyrodinium aureolum Hulburt in culture. *J. Plankton Res.* **13**, 389 (1991). doi:10.1093/plankt/13.2.389

124. A. Larsen, S. Bryant, Growth rate and toxicity of Prymnesium parvum and Prymnesium patelliferum (Haptophyta) in response to changes in salinity, light and temperature. *Sarsia* **83**, 409 (1998).

125. D. S. Reay, D. B. Nedwell, J. Priddle, J. C. Ellis-Evans, Temperature dependence of inorganic nitrogen uptake: reduced affinity for nitrate at suboptimal temperatures in both algae and bacteria. *Appl. Environ. Microbiol.* **65**, 2577 (1999). Medline

126. E. Nordli, Experimental studies on the ecology of Ceratia. *Oikos* **8**, 200 (1957). doi:10.2307/3564999

127. M. Montresor, C. R. Tomas, Growth and probably gamete formation in the marine dinoflagellate Ceratium schrankii. *J. Phycol.* **24**, 495 (1988).

128. G. Mjaaland, Some laboratory experiments on the coccolithophorid Coccolithus huxleyi. *Oikos* **7**, 251 (1956). doi:10.2307/3564925

129. C. Lovejoy *et al*., Distribution, phylogeny, and growth of cold-adapted picoprasinophytes in Arctic seas. *J. Phycol.* **43**, 78 (2007). doi:10.1111/j.1529-8817.2006.00310.x

130. Z. I. Johnson *et al*., Niche partitioning among Prochlorococcus ecotypes along ocean-scale environmental gradients. *Science* **311**, 1737 (2006). doi:10.1126/science.1118052 Medline

131. A. R. Juhl, Growth rates and elemental composition of Alexandrium monilatum, a red-tide dinoflagellate. *Harmful Algae* **4**, 287 (2005). doi:10.1016/j.hal.2004.05.003

132. E. R. Zinser *et al*., Influence of light and temperature on Prochlorococcus ecotype distributions in the Atlantic Ocean. *Limnol. Oceanogr.* **52**, 2205 (2007). doi:10.4319/lo.2007.52.5.2205

133. B. J. Binder, D. M. Anderson, Physiological and environmental control of germination in Scripsiella trochoidea (Dinophyceae) resting cysts. *J. Phycol.* **23**, 99 (1987).

134. H. Kaeriyama *et al*., Effects of temperature and irradiance on growth of strains belonging to seven Skeletonema species isolated from Dokai Bay, southern Japan. *Eur. J. Phycol.* **46**, 113 (2011). doi:10.1080/09670262.2011.565128

135. J. Navarro, M. Munoz, A. Contreras, Temperature as a factor regulating growth and toxin content in the dinoflagellate Alexandrium catenella. *Harmful Algae* **5**, 762 (2006). doi:10.1016/j.hal.2006.04.001